NAVAL AIR WARFARE CENTER AIRCRAFT DIVISION
PATUXENT RIVER, MARYLAND

TECHNICAL REPORT

REPORT NO: NAWCADPAX--99-221-TR

MECHANICAL PROPERTIES OF Be-Al ALLOYS

by

E. U. Lee
K. George
V. V. Agarwala
H. Sanders

22 February 2000

Aerospace Materials Division
Air Vehicle Department
Naval Air Warfare Center Aircraft Division
Patuxent River, Maryland

Approved for public release; distribution is unlimited.

DEPARTMENT OF THE NAVY
NAVAL AIR WARFARE CENTER AIRCRAFT DIVISION
PATUXENT RIVER, MARYLAND

NAWCADPAX--99-221-TR
22 February 2000

RELEASED BY:

Wm Frazier 2/22/00
WILLIAM E. FRAZIER / DATE
Head, Metals and Ceramics Branch

Dale F. Moore 2/22/00
DALE MOORE / DATE
Director, Materials Competency
Naval Air Warfare Center Aircraft Division

REPORT DOCUMENTATION PAGE

Form Approved
OMB No. 0704-0188

1. REPORT DATE	2. REPORT TYPE	3. DATES COVERED
22 February 2000	Technical Report	26 December 1996 - 30 September 1998

4. TITLE AND SUBTITLE

Mechanical Properties of Be-Al Alloys

5a. CONTRACT NUMBER

5b. GRANT NUMBER

5c. PROGRAM ELEMENT NUMBER

6. AUTHOR(S)

E. U. Lee
K. George
V. V. Agarwala
H. Sanders

5d. PROJECT NUMBER

5e. TASK NUMBER

5f. WORK UNIT NUMBER

7. PERFORMING ORGANIZATION NAME(S) AND ADDRESS(ES)

Naval Air Warfare Center Aircraft Division
22347 Cedar Point Road, Unit #6
Patuxent River, Maryland 20670-1161

8. PERFORMING ORGANIZATION REPORT NUMBER

NAWCADPAX--99-221-TR

9. SPONSORING/MONITORING AGENCY NAME(S) AND ADDRESS(ES)

Defense Advanced Research Project Agency
3701 North Fairfax Drive
Arlington, Virginia 22203-1714

10. SPONSOR/MONITOR'S ACRONYM(S)

11. SPONSOR/MONITOR'S REPORT NUMBER(S)

12. DISTRIBUTION/AVAILABILITY STATEMENT

Approved for public release; distribution is unlimited.

13. SUPPLEMENTARY NOTES

14. ABSTRACT

This study was conducted to define the mechanical properties of a wrought 62Be-38A1 alloy and a cast 65Be-32A1-3NI alloy. The tensile strength and elongation were measured at room temperature, 66°C (150°F), 121°C (250°F), 177°C (350°F), and 232°C (450°F). The fracture toughness was determined at room temperature. The fatigue behavior was characterized in terms of stress-life (S-N) and crack growth rate - stress intensity range (da/dN-ΔK) relations at room temperature. The microstructure was examined, and the crack path was identified for each mechanical testing.

15. SUBJECT TERMS

Mechanical Property
Wrought Alloy
Fracture Toughness
Fatigue Crack Growth
Stress Intensity Range
Microstructure

16. SECURITY CLASSIFICATION OF:			17. LIMITATION OF ABSTRACT	18. NUMBER OF PAGES	19a. NAME OF RESPONSIBLE PERSON
a. REPORT	b. ABSTRACT	c. THIS PAGE			Eun Lee
Unclassified	Unclassified	Unclassified	UL	44	19b. TELEPHONE NUMBER (include area code) 301-342-8069

ABSTRACT

This study was conducted to define the mechanical properties of a wrought 62Be-38Al alloy and a cast 65Be-32Al-3Ni alloy. The tensile strength and elongation were measured at room temperature, 66°C (150°F), 121°C (250°F), 177°C (350°F), and 232°C (450°F). The fracture toughness was determined at room temperature. The fatigue behavior was characterized in terms of stress-life (S-N) and crack growth rate - stress intensity range (da/dN-ΔK) relations at room temperature. The microstructure was examined, and the crack path was identified for each mechanical testing.

CONTENTS

ACKNOWLEDGMENT

This study was supported by the Defense Advanced Research Project Agency, ARPA Order No. E774-01. Special thanks are due to Dr. Gilbert London for monitoring this contract study and providing technical guidance.

SUMMARY

The microstructure of the wrought and cast alloys consists of Be-phase particles and Al-phase matrix. The Be-phase particles are aligned along the rolling direction in the wrought alloy; whereas, they are coarser and round with no directionality in the cast alloy. Overall, the wrought alloy has better mechanical properties, including fatigue resistance, than the cast alloy. The conditional plane strain fracture toughnesses of the wrought alloy are 38.8 and 22.4 MPa$\sqrt{m}$ (35.3 and 20.4 ksi$\sqrt{in}$) for L-T and T-L orientations at room temperature, respectively. During tensile testing at room temperature, the fracture cuts through the Be- and Al-phase in the cast alloy. However, the crack path follows preferentially the Al-phase and the Al/Be interfacial region at all temperatures in the wrought alloy and at higher temperatures in the cast alloy during tensile, fracture-toughness, and fatigue testing.

INTRODUCTION

High specific modulus aerospace structures should have low density and good thermal conductivity to resist aeroelastic vibration, deformation, and high heat loads. Additional performance requirements are becoming necessary with advanced supersonic and hypersonic designs. These include high fracture toughness, fatigue resistance, strength, and ductility to eliminate or minimize the possibility of catastrophic fracture and fatigue failure, and to facilitate the weight saving and fabrication. Several material systems have been investigated for their capability in meeting the stringent combination of requirements, including titanium aluminide intermetallic compounds, metal matrix composites, and beryllium. These materials, however, proved to be deficient in their capability to meet the fracture toughness and fatigue resistance requirements. Thus, an alloy system, combining beryllium's attributes of low density, high strength, and high modulus with aluminum's low temperature toughness, is a viable candidate material.

Among the attributes of beryllium are its low density of 1.85 g/cm^3 (0.067 lb/in.^{3}) and high elastic modulus of 276 to 303 GPa (40×10^6 to 44×10^6 psi). The density is approximately two-thirds that of aluminum and one-fourth that of steel. This gives beryllium a specific modulus 6.6 times greater than those of aluminum, steel, magnesium, and some titanium alloys. However, beryllium has several drawbacks for its use as an aircraft material. The fracture toughness of the consolidated beryllium powder metallurgy product is lower than that of most materials, typically 7.7 to 12.1 MPa$\sqrt{m}$ (7 to 11 ksi$\sqrt{in}$.). In addition, beryllium cannot be welded by conventional means. Alloying with aluminum can improve the fracture toughness, and allows fabrication and repair of components by fusion welding.

Beryllium-aluminum alloys have shown a potential for overcoming the deficiencies of beryllium. The limit of aluminum concentration of such alloys must be considered because of the increased density, reduced strength, and reduced modulus associated with the dilution of beryllium. The alloys, which have undergone the most intensive prior evaluation, generally in the region of 30 to 40% aluminum (reference 1), have improved ductility and a more forgiving failure mode. The composition of 62Be-38Al is the alloy which has had the greatest attention within the aircraft structural alloy community (references 2 through 5). Other investigations have concentrated upon

modifications incorporating either greater aluminum content or the addition of ternary alloying elements, most notably 53Be-47Al (LX-53) and 59Be-38Al-3Mg (LX59-3). The improvement in room temperature elongation, associated with a higher aluminum content, was accompanied with decreased strength and modulus and increased density. The use of a ternary alloying element in a lower beryllium content alloy has appeared to improve yield strength, ultimate tensile strength, and elongation.

Evaluations performed in the 1960's and 1970's focused on the attributes of uniform and fine microstructure provided by powder metallurgy (PM) technology. Investigations prior to the PM work revolved around ingot metallurgy (IM) technology (sand and mold casting) producing a coarse dendritic structure that did not produce mechanical properties appropriate for structural components (reference 1). A development and evaluation program at Brush Wellman, Inc., reinvestigated the capability to manufacture wrought Be-Al alloys using both IM and PM in the late 1980's. A few years ago, Brush Wellman, Inc., conducted a study on casting of Be-Al alloys, including 65Be-32Al-3Ni alloy, under the Navy contract N62269-96-C-0011, Manufacturing Development of Aluminum-Beryllium Investment Cast Alloys for Propulsion Systems. An investigation of the mechanical properties of Be-Al alloy casting was required for the intended application.

This study was initiated to define the mechanical properties of a representative wrought alloy, 62Be-38Al, and a newly developed cast alloy, 65Be-32Al-3Ni.

EXPERIMENTAL PROCEDURE

The specimen materials, plates of a wrought 62Be-38Al alloy and a bearing housing casting of a 65Be-32Al-3Ni alloy, figure A-1, were purchased from Brush Wellman, Inc. The chemical compositions are shown in tables 1 and 2.

Table 1: Chemical Composition of Wrought 62Be-38Al Alloy

Element	Al	Be	O	C	Other Elements, Each
Weight (%)	38.22	61.2	0.24	0.057	0.2 Max

Table 2: Chemical Composition of Cast 65Be-32Al-3Ni Alloy

Element	Al	Be	Ni	C	Cd	Fe
Weight (%)	36.0	60.6	2.9	0.06	0.2	0.3

The specimen materials were machined into rectangular and round tension and fatigue test specimens, figures A-2 and A-3, and compact tension specimens, figure A-4.

Two closed-loop servo-hydraulic MTS mechanical test machines of 100 KN (20 kip) were employed for the tension, fracture toughness, and fatigue tests. For those tests, each machine was monitored and controlled by a computer. The tension test was carried out with a constant crosshead speed of 0.254 mm/min (0.01 in./min) at room temperature, 66°C (150°F), 121°C (250°F), 177°C (350°F), and 232°C (450°F) in laboratory atmosphere. The fracture toughness test was conducted at room temperature, following ASTM Standard E 1820-96 and using a compact tension specimen. The stress-life (S-N) fatigue test was performed under force controlled constant amplitude axial loading of stress ratio 0.1 and frequency 30 Hz at room temperature in laboratory atmosphere. The specimens for this test were rectangular and round fatigue test specimens with a continuous radius between ends. The fatigue crack growth test was conducted under constant amplitude sine wave loading at a frequency of 30 Hz and stress ratios, ranging from 0.1 to 0.6, at room temperature in laboratory atmosphere. In this test, using a compact tension specimen, the crack length was continuously monitored by compliance measurement technique. The near-threshold crack growth rate was obtained under decreasing stress intensity K (load shedding) condition with K-gradient parameter $C = -0.16\ mm^{-1}$.

Metallography was performed on the specimen materials, before and after each mechanical test, to reveal the microstructure. In addition, the fracture surface of the specimens was examined under a Scanning Electron Microscope, JEOL JSM-5800LV, operating at a 20 kV accelerating voltage. The corresponding fracture path was also identified with an optical microscope.

RESULTS AND DISCUSSION

MICROSTRUCTURE

The microstructures of the wrought and cast alloys are shown in figures A-5(a)-(c). The dark structure is Be-phase and the light one Al-phase matrix. In the wrought alloy, the Be-phase particles are not deformed and are aligned along the rolling direction, resulting in banding, figure A-5(a). On the other hand, they are coarser and round or partly equiaxed with no directionality in the cast alloy, figures A-5(b) and (c).

TENSILE PROPERTIES

The tensile test results are summarized for the wrought and cast alloys in table 3. The stress-strain curves are shown for various test temperatures and loading orientations in figures A-6 to A-13. The yield strength (YS) and ultimate tensile strength (UTS) are greater with lower test temperature, and the wrought alloy possesses superior strength and ductility relative to the cast alloy. In the wrought alloy, the YS and UTS are greater for L-orientation than for T-orientation below 177°C (350°F), but the reverse seems to be true above 177°C (350°F).

Table 3: Tensile Properties

Orientation	Temperature °C	Temperature °F	YS MPa	YS ksi	UTS MPa	UTS ksi	Elong %	Modulus GPa	Modulus Msi
Wrought									
L	RT		348.9	50.6	429.5	62.3	8.9	103.4	15.0
	65.6	150	336.5	48.8	406.8	59.0	9.2	124.1	18.0
	121.1	250	299.9	43.5	344.7	50.0	10.0	137.9	20.0
	176.7	350	276.5	40.1	299.2	43.4	8.3	95.1	13.8
	232.2	450	251.0	36.4	260.6	37.8	7.1	63.4	9.2
T	RT		330.9	48.0	413.7	60.0	8.7	120.7	17.5
	65.6	150	325.4	47.2	388.2	56.3	7.1	104.8	15.2
	121.1	250	303.4	44.0	344.7	50.0	7.1	112.4	16.3
	176.7	350	284.8	41.3	306.1	44.4	7.8	113.1	16.4
	232.2	450	251.7	36.5	264.1	38.3	7.3	72.4	10.5
Cast	RT		142.0	20.6	173.1	25.1	3.1	37.2	5.4
	65.6	150	154.4	22.4	175.8	25.5	-	49.6	7.2
	121.1	250	137.9	20.0	146.2	21.2	3.6	32.4	4.7
	176.7	350	103.4	15.0	114.5	16.6	-	29.0	4.2
	232.2	450	96.5	14.0	99.3	14.4	4.0	43.4	6.3

The fracture paths in the etched longitudinal and transverse sections through the fracture surfaces are shown for the wrought and cast alloys in figures A-14 to A-22. In the wrought alloy, the fracture surface is nearly perpendicular to the loading direction and planar at room temperature, figure A-14. The fracture occurs partly through the Be-phase and partly through the Al-phase and the Al/Be interfacial region at room temperature. On the other hand, the fracture surface is wavy, and the fracture path follows more preferentially the Al-phase and the Al/Be interfacial region at higher testing temperatures, figures A-16 to A-19. Such a fracture path feature is seen for both L- and T-orientations. In the cast alloy, the fracture surface is slanted to the loading direction, and the fracture cuts through the Be- and Al-phases at room temperature, figure A-20. However, the fracture path follows more preferentially the Al-phase and Al/Be interfacial region at higher testing temperatures, figures A-21 and A-22.

FRACTURE TOUGHNESS

The conditional plane strain fracture toughness K_Q of the wrought alloy is 38.8 and 22.4 MPa$\sqrt{m}$ (35.3 and 20.4 ksi$\sqrt{in}$) for L-T and T-L orientations at room temperature, respectively.

The fracture path is shown in the micrograph of a side face through the fracture surface for the wrought alloy specimens of L-T and T-L orientations, respectively, figure A-23. The fracture propagates through mostly Al-phase and Al/Be interfacial region for both orientations.

The fracture surfaces are shown for the fracture-toughness-tested wrought alloy specimens of L-T and T-L orientations in figure A-24. From the left edge in figure A-24, in sequence, are the machined notch, the fatigue-precracked zone, and radial zone. The fractographic features of the radial zone, revealed by light microscopy, are coarse radial ridges and marks for the L-T orientation and fine radial marks for the T-L orientation. The radial ridges and marks run parallel to the direction of crack growth, and a ridge is created when two noncoplanar cracks are connected by tearing of the intermediate material. This difference in light microscopy fractographic feature between the L-T and T-L orientations must be associated with the large difference in the fracture toughness.

The corresponding SEM fractographs and X-ray mapping for Be and Al are shown in figures A-25 and A-26. Cleavage facets are observable in the Be-phase and dimples of various sizes in the Al-phase. This observation evidences that the Be-phase fails by cleavage fracture and the Al-phase by ductile dimple fracture.

FATIGUE BEHAVIOR

The results of the stress-life fatigue test, S-N curves, are shown for the rectangular and round specimens of the wrought and cast alloys in figures A-27(a) and (b), respectively. The wrought alloy has much greater fatigue resistance than the cast alloy. In the wrought alloy, the L-orientation loading results in slightly better fatigue resistance than the T-orientation loading.

The results of fatigue crack growth test are exhibited in figures A-28 to A-34. The threshold stress intensity range ΔK_{th} is greater and the fatigue crack growth rate da/dN is lower for orientation L-T than for T-L at stress ratio R = 0.1, figure A-28. On the other hand, the ΔK_{th} is similar for both orientations, but da/dN is smaller for the L-T orientation than for the T-L orientation at R = 0.6, figure A-29. For the cast alloy, the ΔK_{th} is 11.1 MPa$\sqrt{m}$ (10.1 ksi$\sqrt{in.}$), which is much greater than those for the wrought alloy and da/dN increases very steeply, compared to that for the wrought alloy, figure A-30. This indicates that the threshold crack growth resistance of the cast alloy is superior, but its resistance to the subsequent fatigue crack growth is inferior to the wrought alloy. Figures A-31 and A-32 indicate that raising stress ratio R increases the near-threshold fatigue crack growth rate and reduces the ΔK_{th} for the wrought alloy specimens of L-T orientation. The variation of ΔK_{th} and maximum stress intensity $K_{max} = \Delta K_{th}/(1-R)$ with R is shown for the wrought alloy specimens of L-T orientation in figure A-33. The ΔK_{th} decreases with increasing R for $R < 0.3$ and levels off for $R > 0.3$. K_{max} changes little for $R < 0.3$, but increases steeply above R = 0.3 with increasing R. The ΔK_{th} is plotted against the K_{max} in figure A-34. Such a curve is called fundamental threshold curve (reference 6), providing interrelation of ΔK_{th} and K_{max}, and defines regions, where fatigue crack grows (above the curve) and where it does not (below the curve). In other words, this curve delineates a boundary where fatigue crack growth starts for a given K_{max} and indicates the resistance to threshold fatigue crack growth.

An example of the fatigue crack path is shown in the micrograph of a section through the fracture surface for wrought and cast alloy specimens in figures A-35 and A-36, respectively. The fatigue crack propagates preferentially through Al-phase and Al/Be interfacial region in wrought and cast alloys.

THIS PAGE INTENTIONALLY LEFT BLANK

CONCLUSIONS

The microstructure of the wrought 62Be-38Al and cast 65Be-32Al-3Ni alloys consists of Be-phase particles and Al-phase matrix. The Be-phase particles are not deformed, and they are aligned along the rolling direction in the wrought alloy. On the other hand, they are coarser and round in the cast alloy.

Overall, the yield strength and ultimate tensile strength are greater with lower test temperature for both the wrought and cast alloys; the wrought alloy has superior strength and ductility compared to the cast alloy.

In the wrought alloy, tensile fracture occurs partly through the Be-phase and partly through the Al-phase and the Al/Be interfacial region at room temperature. The fracture path follows preferentially the Al-phase and the Al/Be interfacial region at higher testing temperatures.

In the cast alloy, tensile fracture cuts through the Be- and Al-phases at room temperature. However, the fracture path follows more preferentially the Al-phase and the Al/Be interfacial region at higher testing temperatures.

The conditional plane strain fracture toughnesses of the wrought alloy are 38.8 and 22.4 MPa$\sqrt{m}$ (35.3 and 20.4 ksi$\sqrt{in.}$) for L-T and T-L orientations at room temperature, respectively.

During the fracture toughness test of the wrought alloy, the fracture propagates through mostly Al-phase and Al/Be interfacial region for both orientations of L-T and T-L. The fracture mode of the Be-phase is cleavage fracture, whereas that of the Al-phase is ductile dimple fracture.

The wrought alloy has much greater fatigue endurance than the cast alloy. In the wrought alloy, L-orientation loading results in slightly better fatigue resistance than the T-orientation loading.

The cast alloy has superior resistance to threshold fatigue crack growth but inferior resistance to the subsequent fatigue crack growth than the wrought alloy.

The fatigue crack propagates preferentially through Al-phase and Al/Be interface region in wrought and cast alloys.

RECOMMENDATION

Conduct a more extensive study on Be-alloys for a thorough understanding of metallurgical characteristics and mechanical behavior of Be-alloys.

THIS PAGE INTENTIONALLY LEFT BLANK

REFERENCES

1. Steinberg, Fenn R., Crooks, D., and Underwood, E., Beryllium-Aluminum Alloy, USP 3, 337, 334, of 22 Aug 1967.

2. Crossley, F. A. and Crooks, D. D., Lockalloy Research and Development, Final Technical Report LMSC-D267216, Lockheed Missiles & Space Co. Inc., Palo Alto, CA, of 1 May 1972.

3. Floyd, D. R. and Lowe, J. N., Beryllium Science and Technology, vol. 2, Plenum Press, New York, NY 1979.

4. Duba, R. J., Haramis, A. C., Marks, R. F., Payne, L., and Sessing, R. C., YF-12 Lockalloy Ventral Fin Program, Final Report NASA CR-144971, Lockheed-California Co., Burbank, CA, of 9 Jan 1976.

5. London, G. J., Beryllium-Aluminum Sheet and Tubing Development Program, NASP Technical Memorandum 1210, Naval Air Warfare Center, Warminster, PA, of Jul 1995.

6. Vasudevan, A. K. and Sadananda, K., Classification of Fatigue Crack Growth Behavior, Metallurgical and Materials Transactions A, 1995, vol. 26A, pp. 12212-1234.

THIS PAGE INTENTIONALLY LEFT BLANK

APPENDIX A
FIGURES

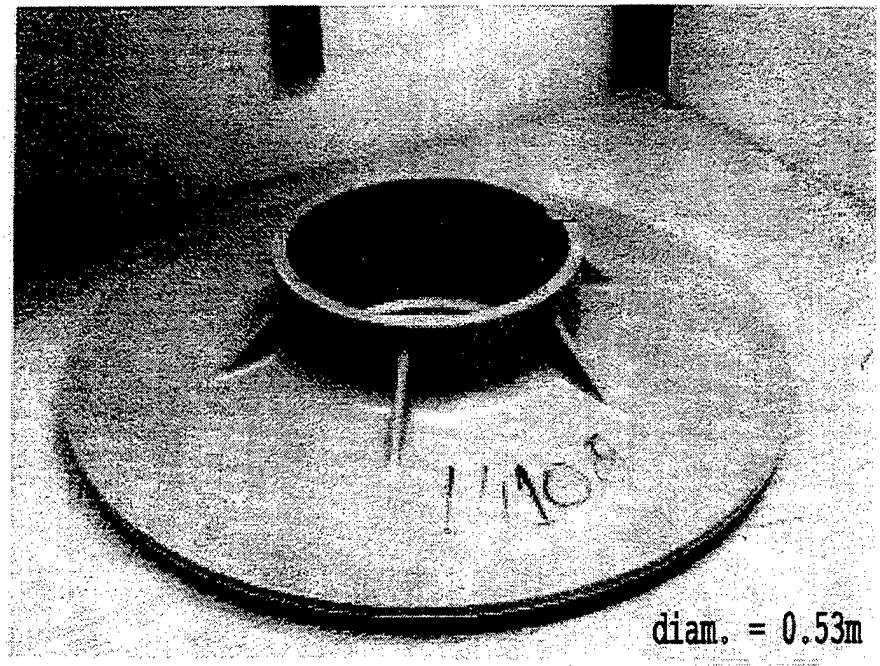

(a) Top

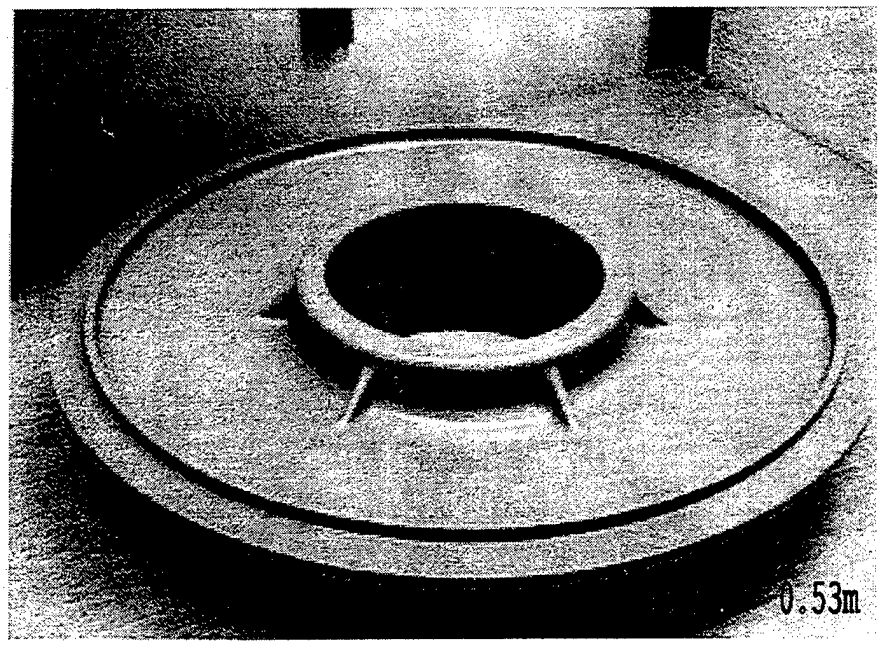

(b) Bottom

Figure A-1: Photographs Showing Top and Underside Views of a Bearing Housing Casting of 65Be-32Al-3Ni Alloy

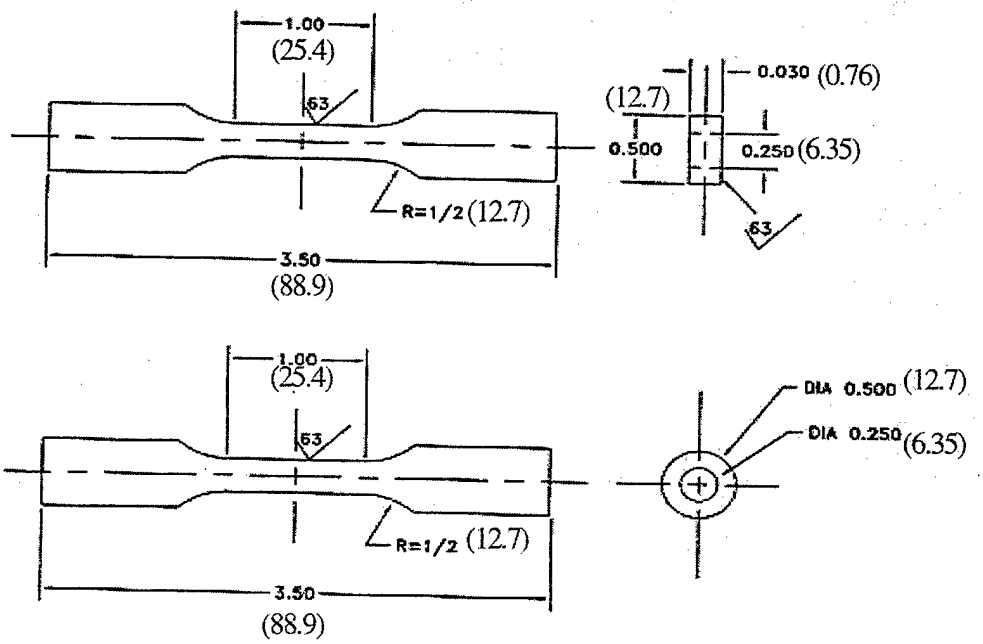

(a) Rectangular and round specimens

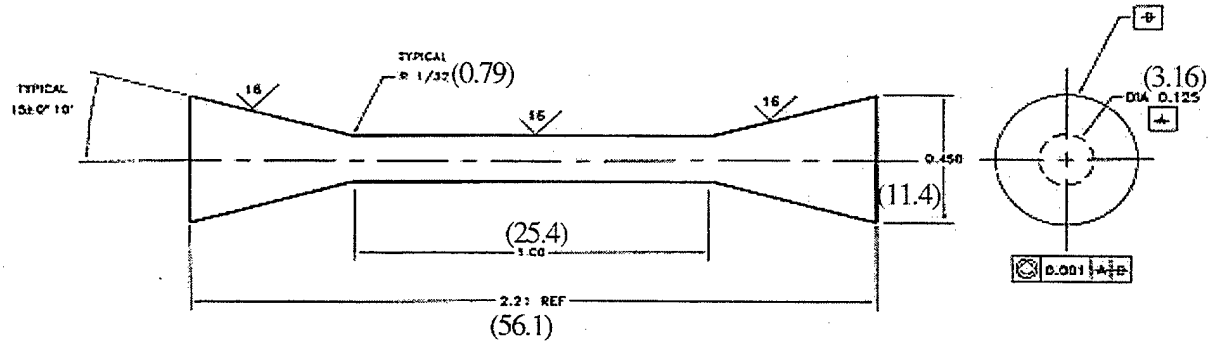

(b) Micro specimen for casting

Figure A-2: Schematics Depicting Tensile Test Specimen Geometries
Note: (mm) SI Units

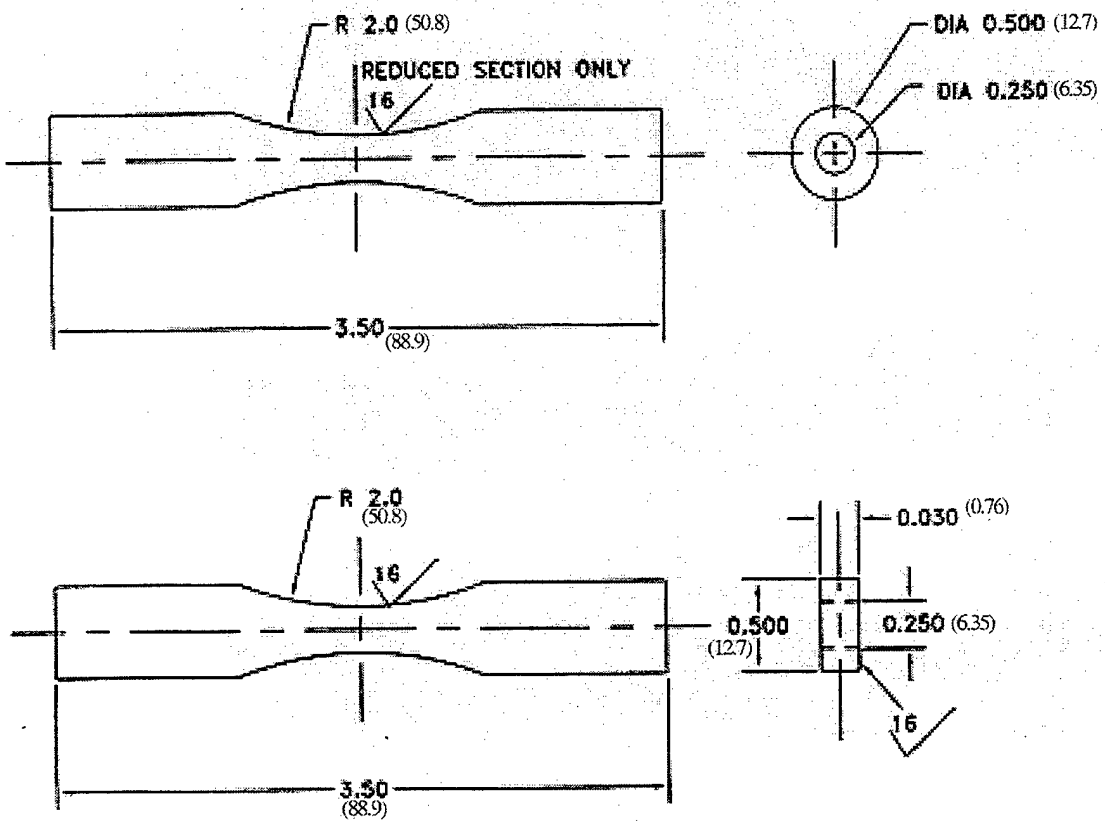

Figure A-3: Schematics Depicting Round and Rectangular Fatigue Test Specimens with a Continuous Radius Between Ends
Note: (mm) SI Units

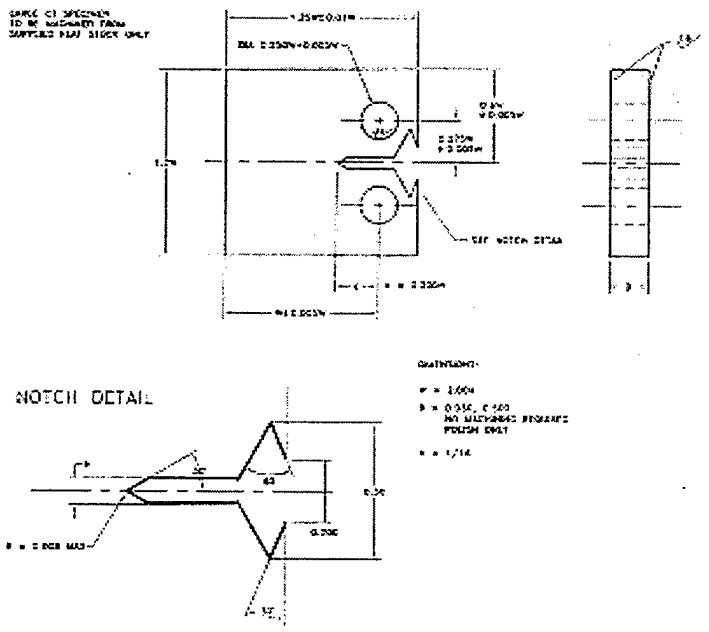

(a) W = 50.8 mm (2 in.)

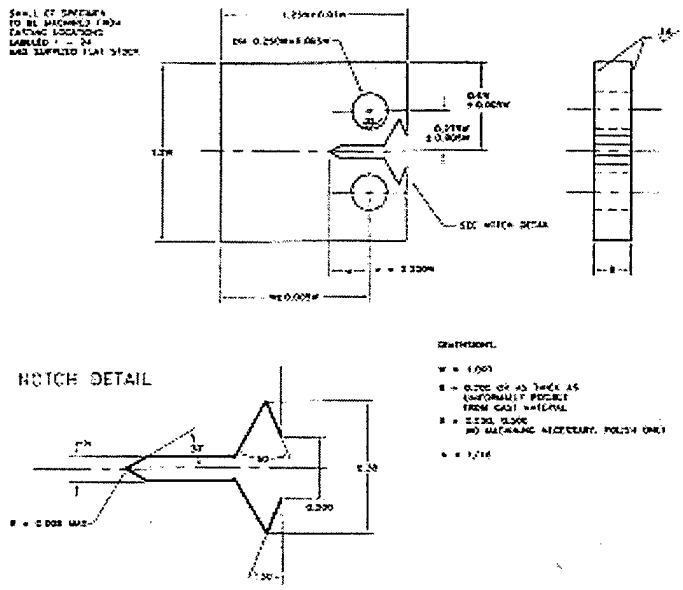

(b) W = 25.4 mm (1 in.)

Figure A-4: Schematics Illustrating Compact Tension Specimen for Fatigue Test

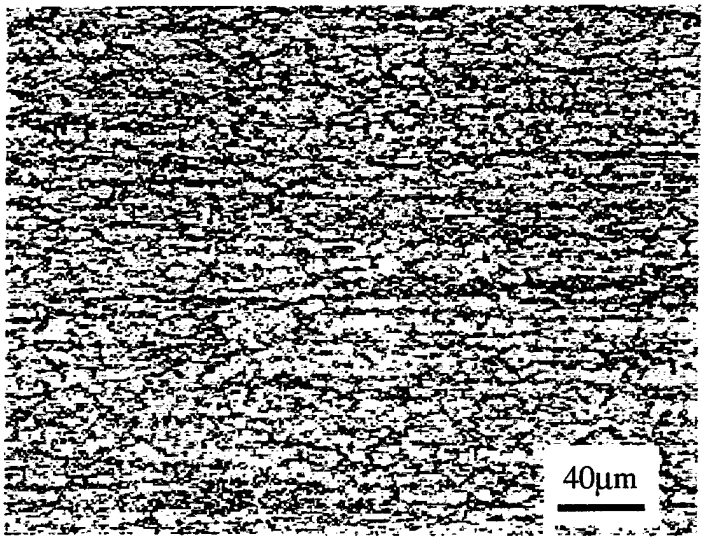

(a) Wrought alloy

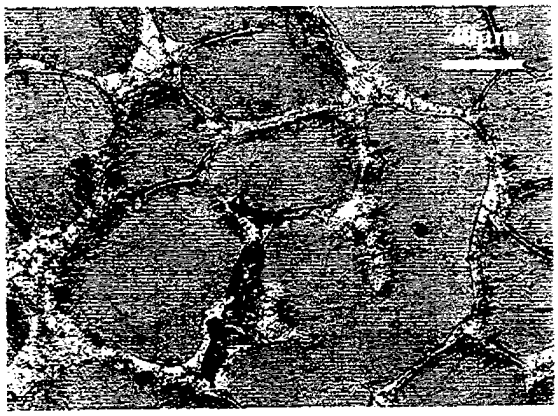

(b) Cast alloy

(c) Cast alloy

Figure A-5: Optical Micrographs Revealing Microstructures of Wrought and Cast Be-Al Alloys

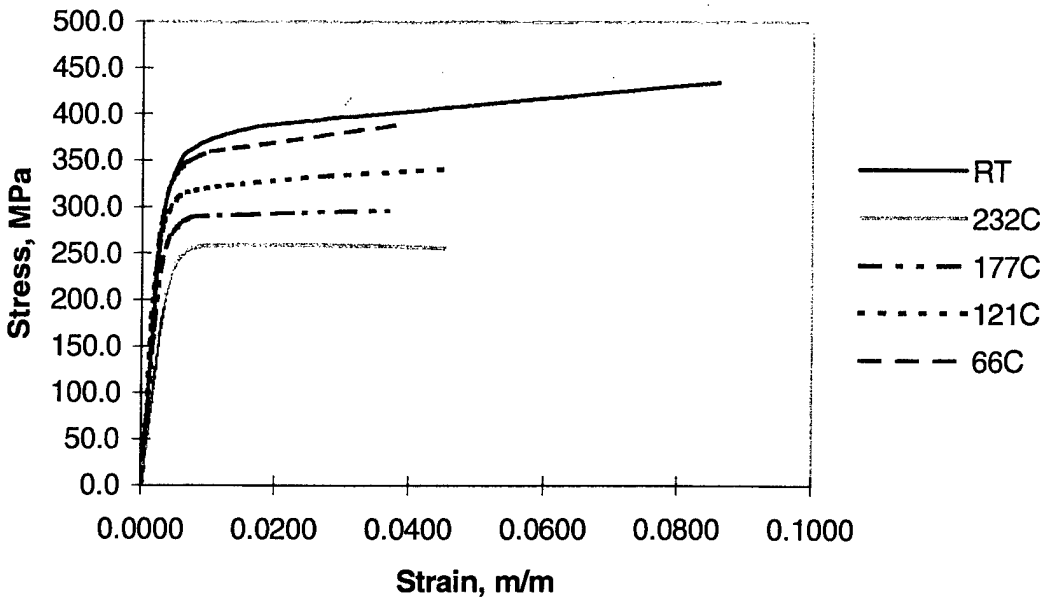

Figure A-6: Stress-Strain Curves for Wrought Be-Al Alloy of L-Orientation at Various Temperatures

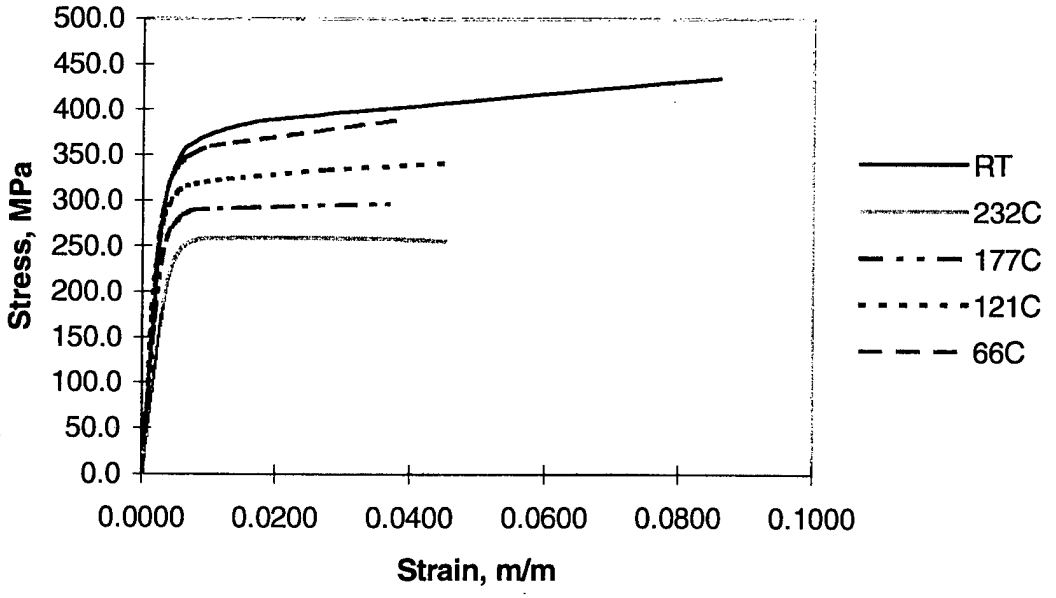

Figure A-7: Stress-Strain Curves for Wrought Be-Al Alloy of T-Orientation at Various Temperatures

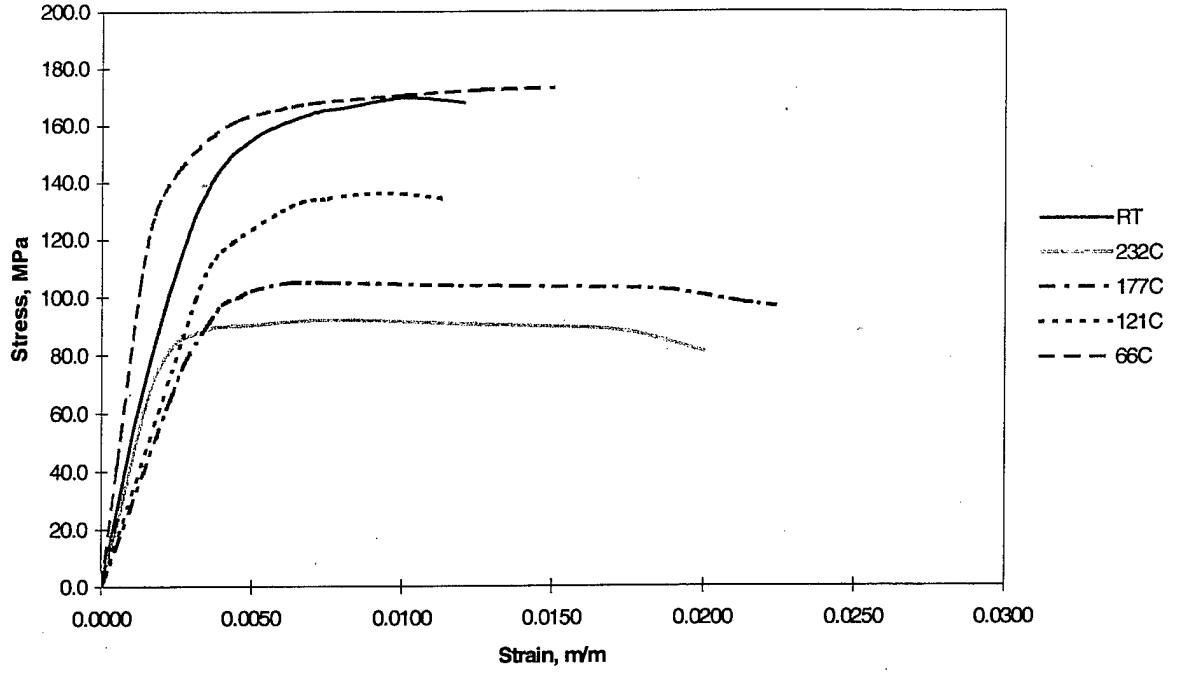

Figure A-8: Stress-Strain Curves for Cast Be-Al Alloy at Various Temperatures

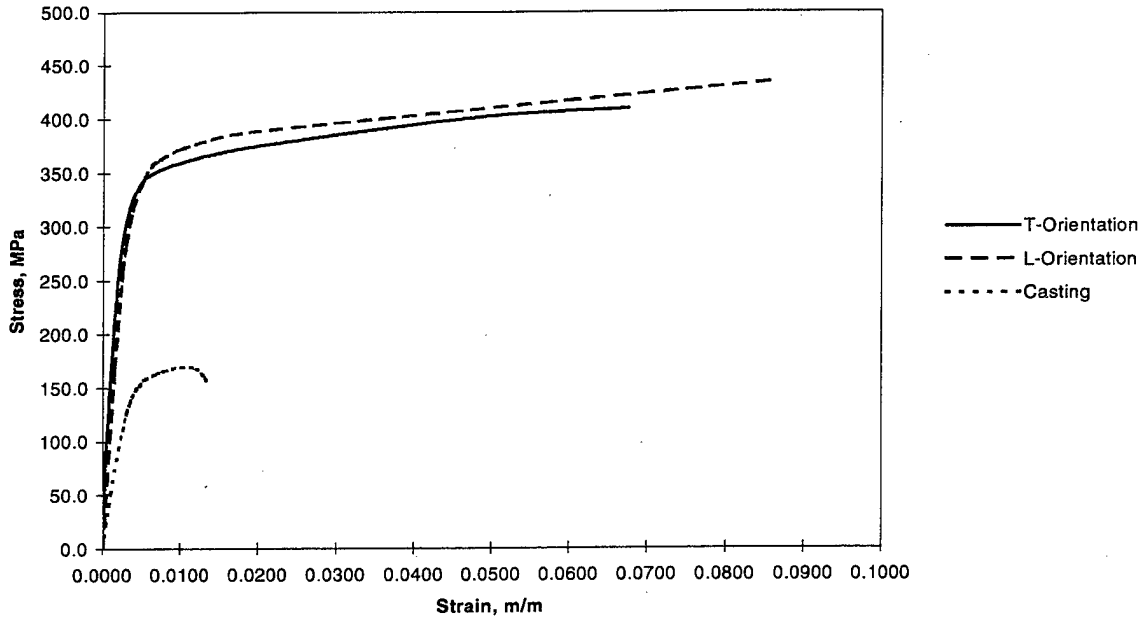

Figure A-9: Stress-Strain Curves for Wrought and Cast Be-Al Alloys at Room Temperature

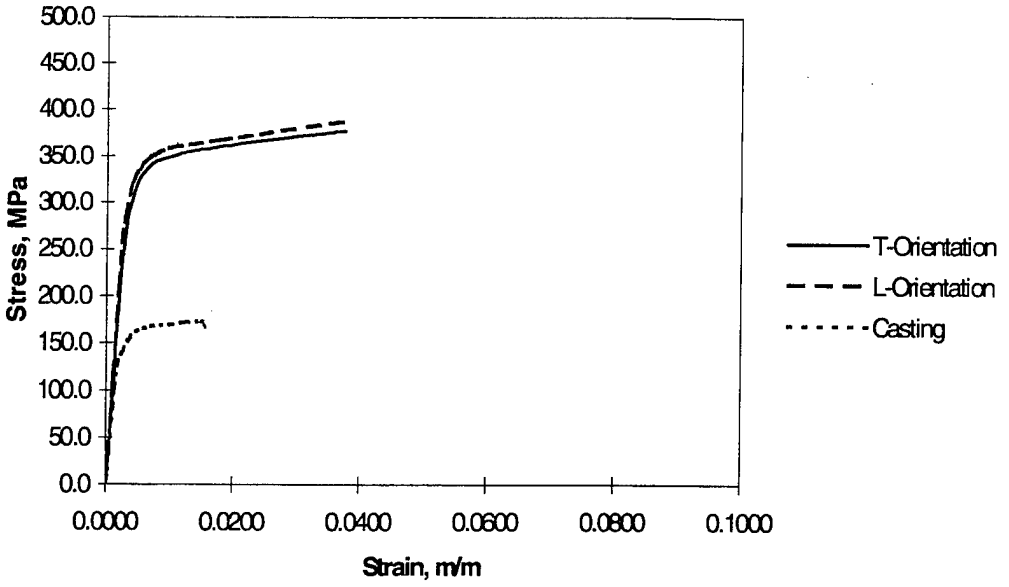

Figure A-10: Stress-Strain Curves for Wrought and Cast Be-Al Alloys at 66°C (150°F)

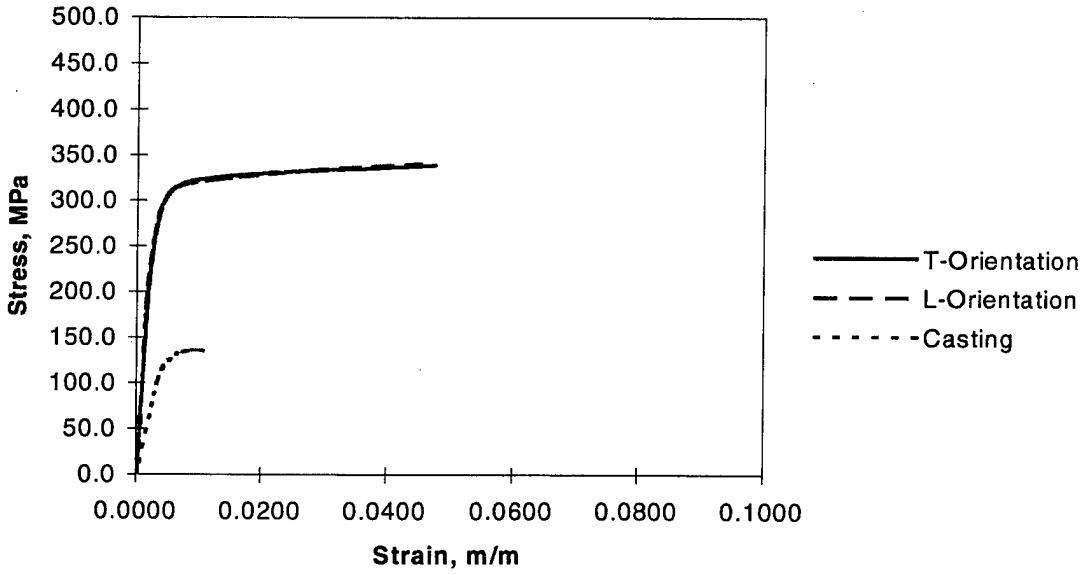

Figure A-11: Stress-Strain Curves for Wrought and Cast Be-Al Alloys at 121°C (250°F)

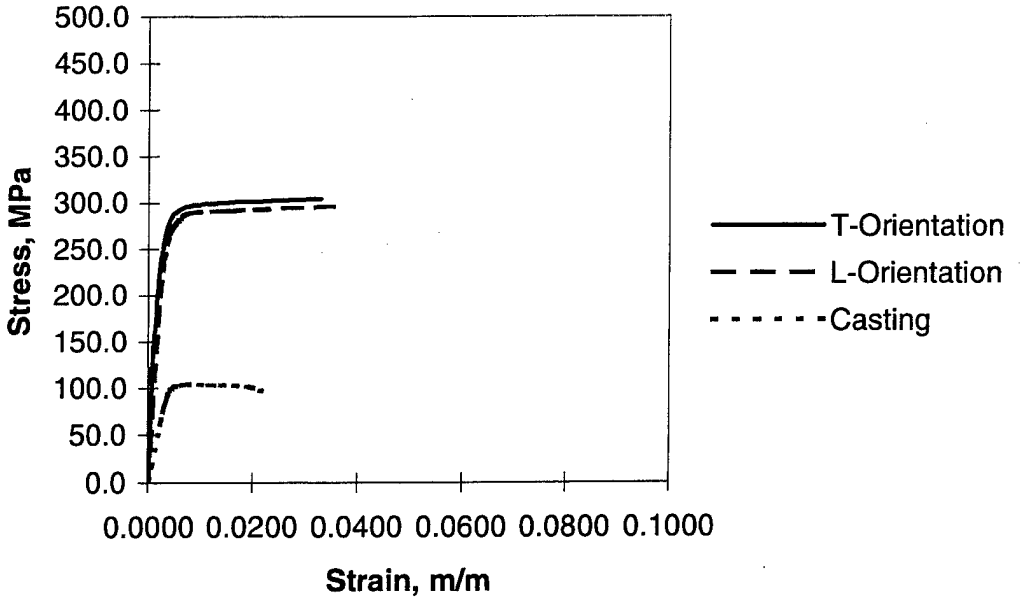

Figure A-12: Stress-Strain Curves for Wrought and Cast Be-Al Alloys at 177°C (350°F)

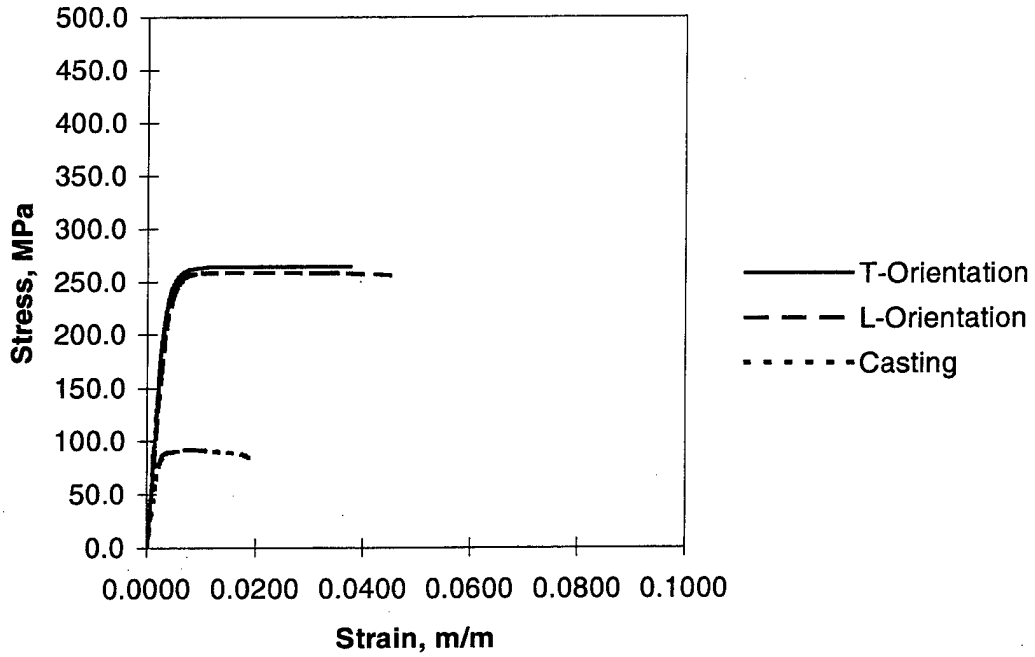

Figure A-13: Stress-Strain Curves for Wrought and Cast Be-Al Alloys at 232°C (450°F)

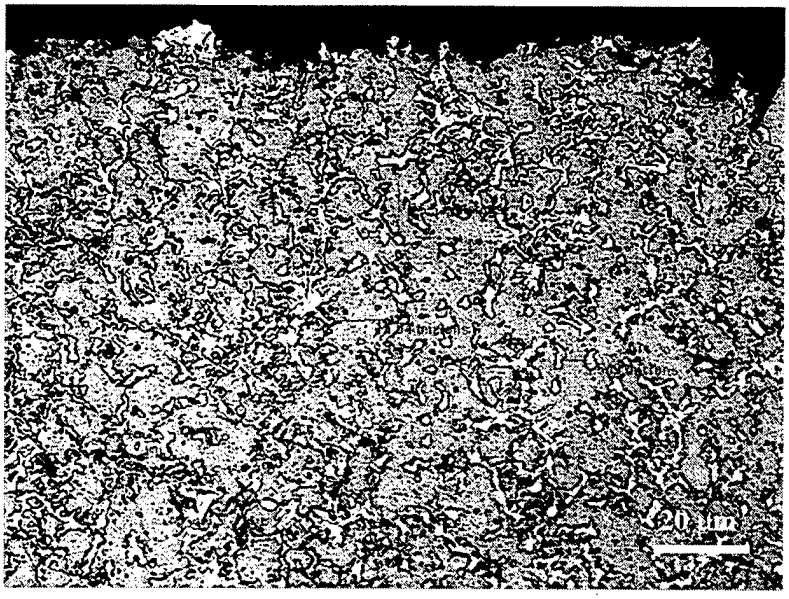

Figure A-14: Optical Micrograph of a Longitudinal Section Through the Fracture Surface Showing the Fracture Path and Microstructure for a Wrought Be-Al Alloy Specimen That Had Been Tensile Tested at Room Temperature

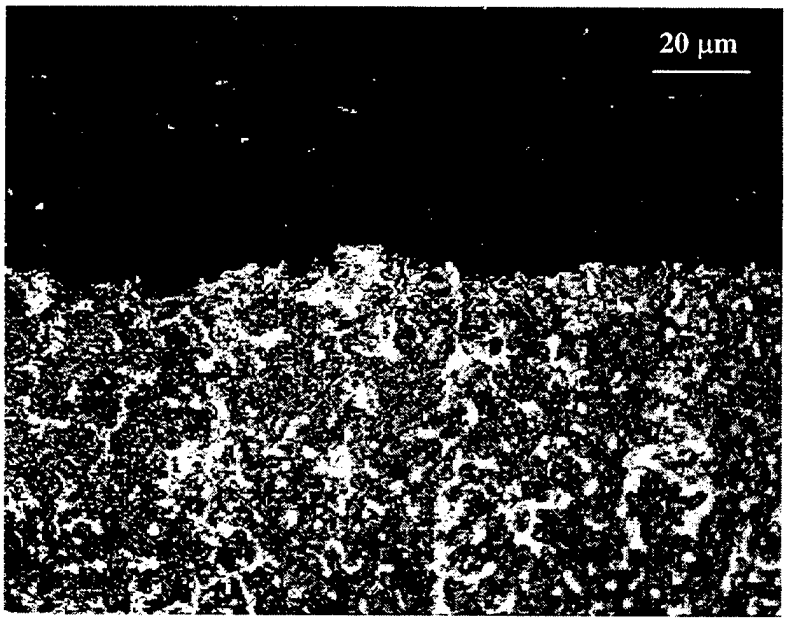

Figure A-15: Optical Micrograph of a Transverse Section Through the Fracture Surface Showing the Fracture Path and Microstructure for a Wrought Be-Al Alloy Specimen That Had Been Tensile Tested at Room Temperature

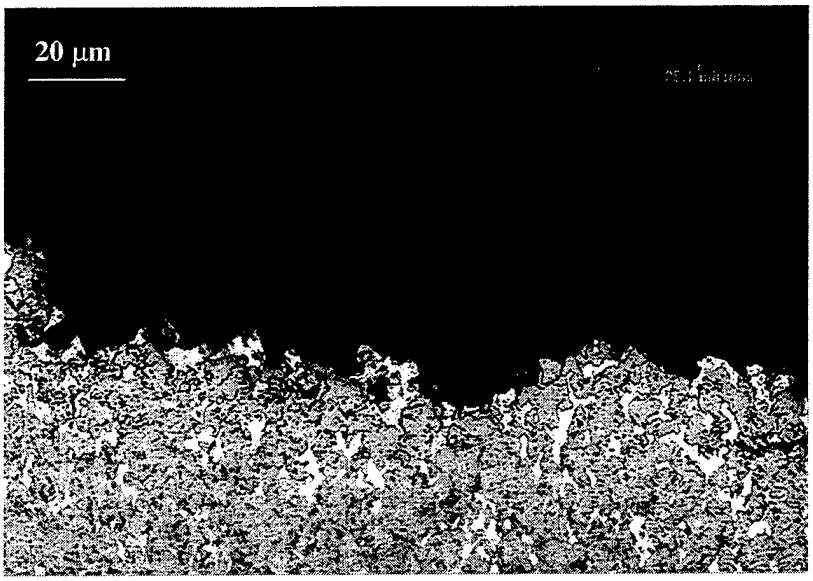

Figure A-16: Optical Micrograph of a Longitudinal Section Through the Fracture Surface Showing the Fracture Path and Microstructure for a Wrought Be-Al Alloy Specimen Tensile Tested at 121°C (250°F)

Figure A-17: Optical Micrograph of a Transverse Section Through the Fracture Surface Showing the Fracture Path and Microstructure for a Wrought Be-Al Alloy Specimen Tensile Tested at 121°C (250°F)

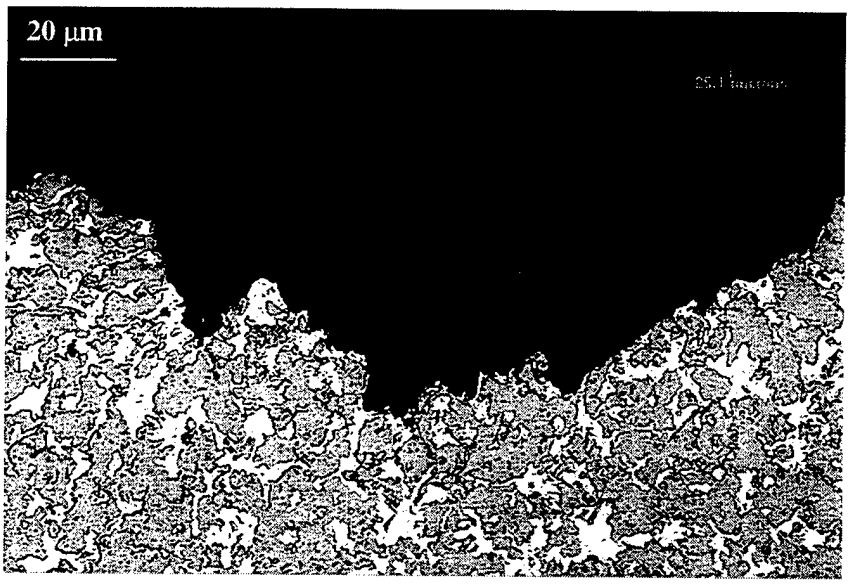

Figure A-18: Optical Micrograph of a Longitudinal Section Through the Fracture Surface Showing the Fracture Path and Microstructure for a Wrought Be-Al Alloy Specimen Tensile Tested at 232°C (450°F)

Figure A-19: Optical Micrograph of a Transverse Section Through the Fracture Surface Showing the Fracture Path and Microstructure for a Wrought Be-Al Alloy Specimen Tensile Tested at 232°C (450°F)

(a)

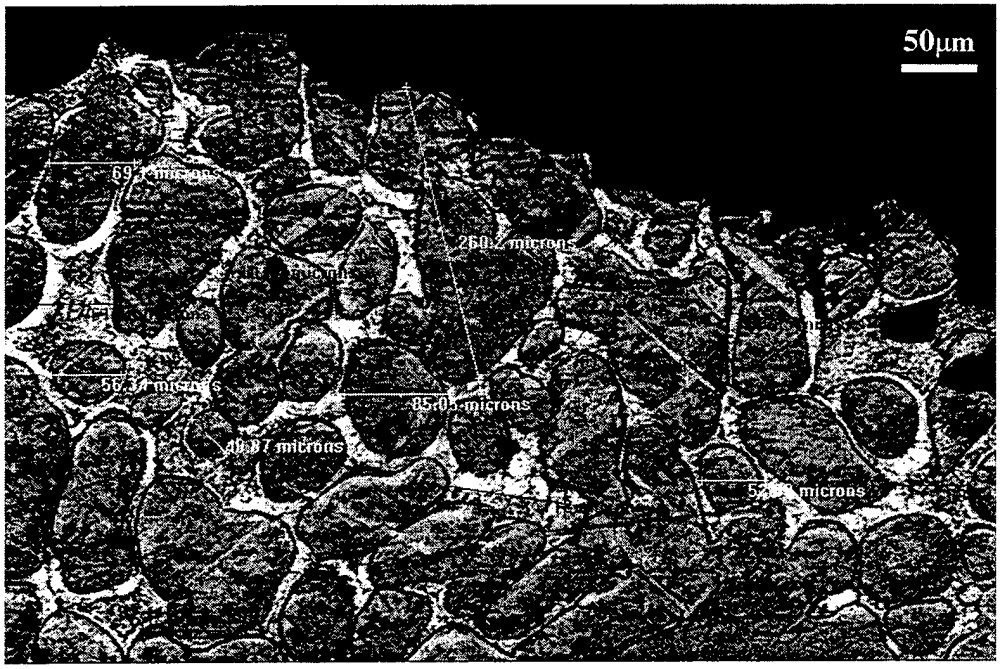

(b)

Figure A-20 (a) and (b): Optical Micrograph of a Section Through the Fracture Surface Showing the Fracture Path and Microstructure for a Cast Be-Al Alloy Specimen Tensile Tested at Room Temperature

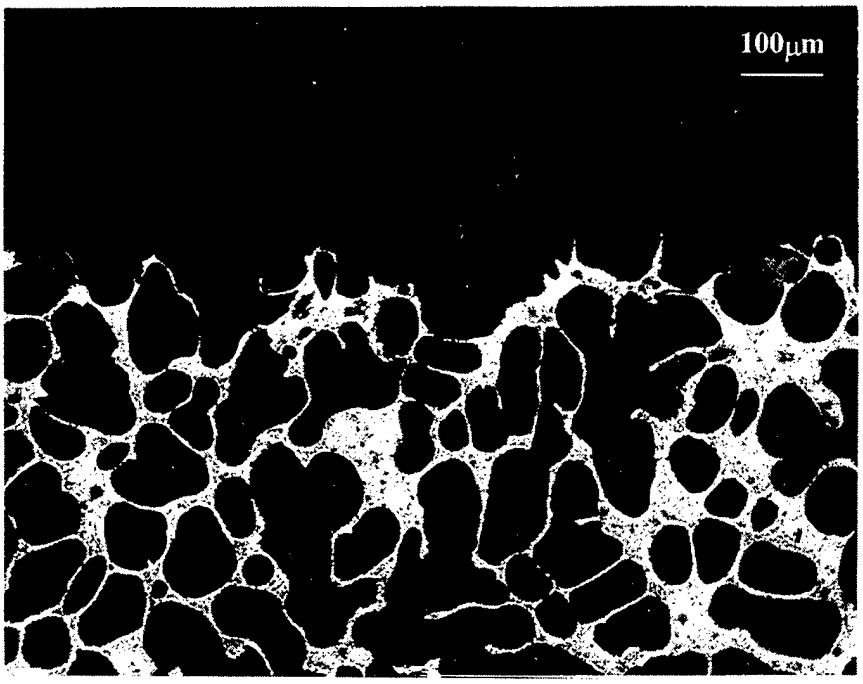

Figure A-21: Optical Micrograph of a Section Through the Fracture Surface Showing the Fracture Path and Microstructure for a Cast Be-Al Alloy Specimen Tensile Tested at 121°C (250°F)

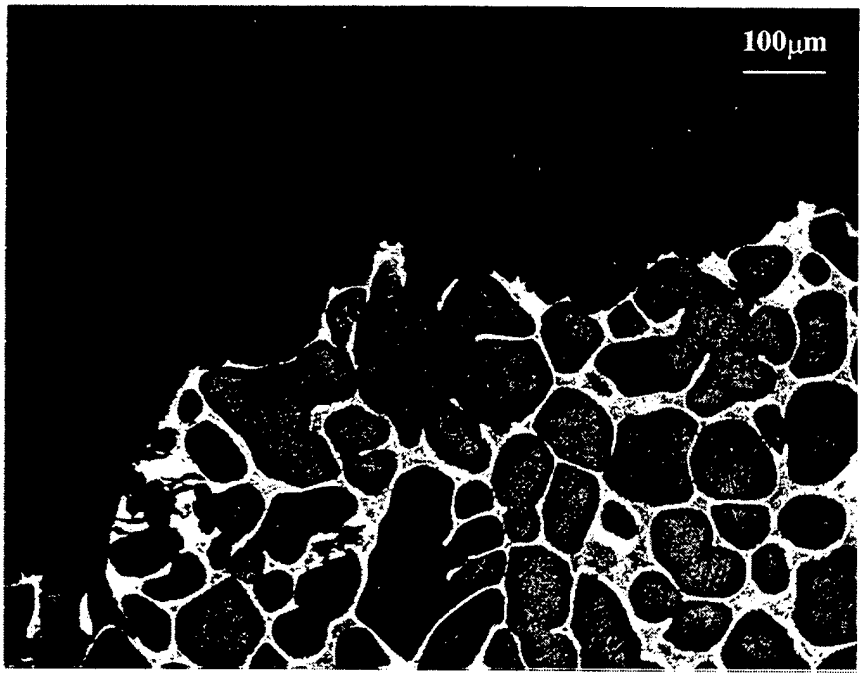

Figure A-22: Optical Micrograph of a Section Through the Fracture Surface Showing the Fracture Path and Microstructure for a Cast Be-Al Alloy Specimen Tensile Tested at 232°C (450°F)

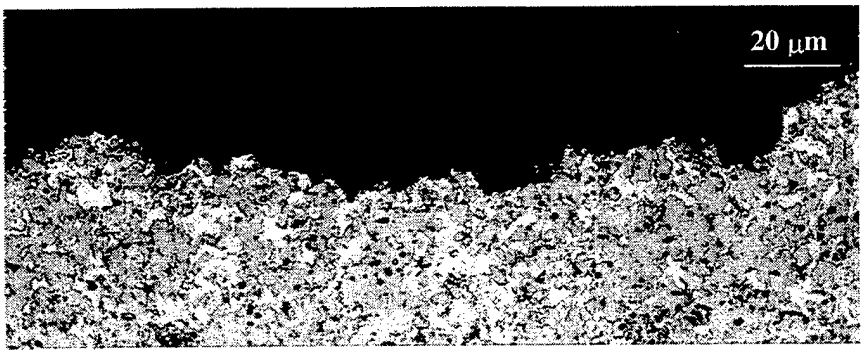

(a) L-T Orientation

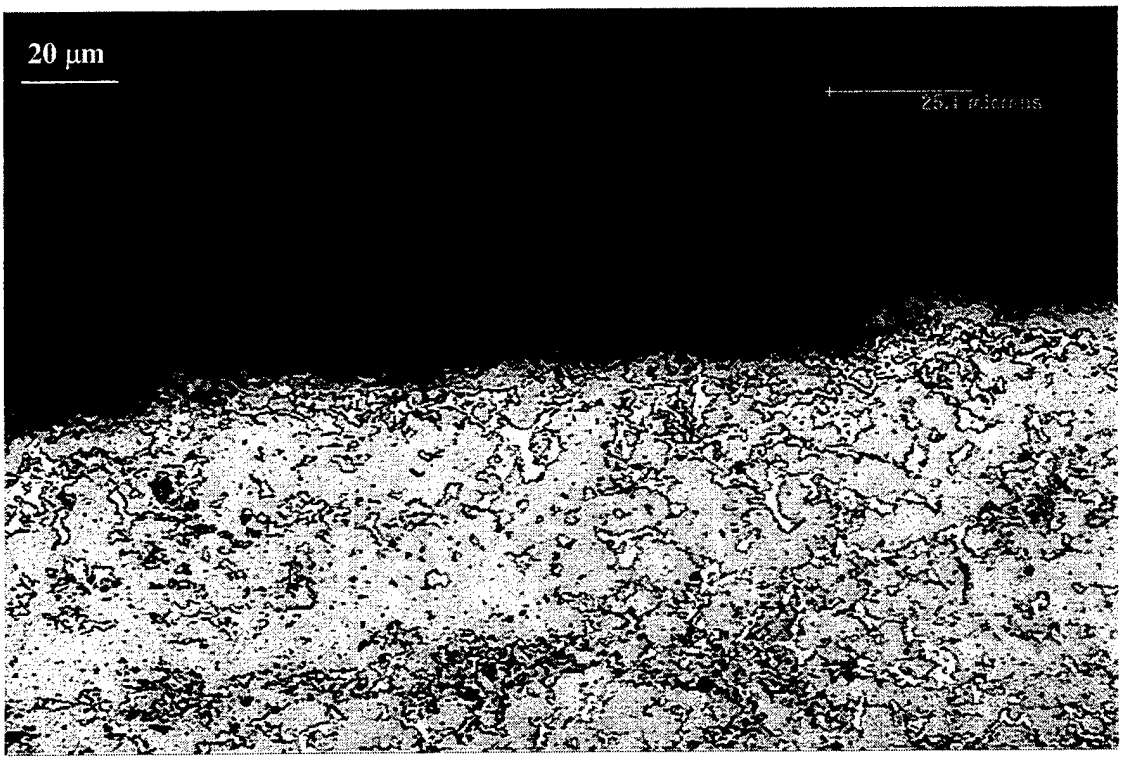

(b) T-L Orientation

Figure A-23: Optical Micrographs of a Section Through the Fracture Surface Showing the Fracture Path and Microstructure for a Wrought Be-Al Alloy Specimen That Had Been Fracture-Toughness Tested at Room Temperature

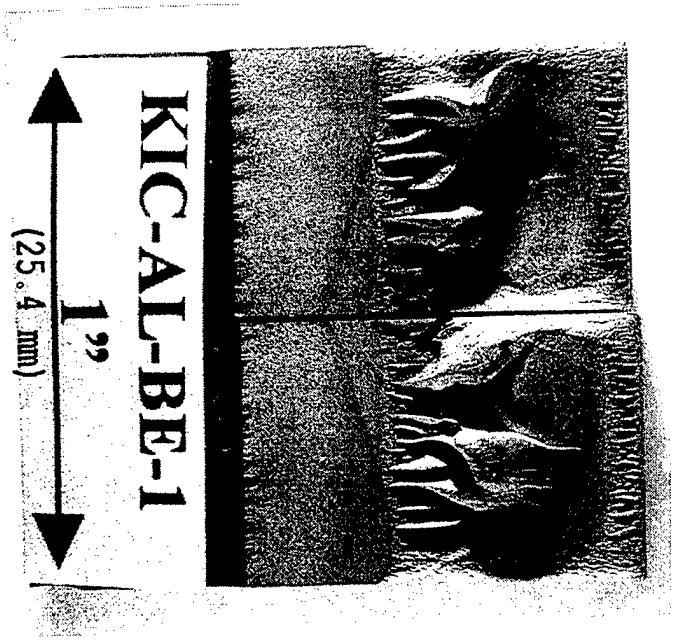

(a) L-T Orientation

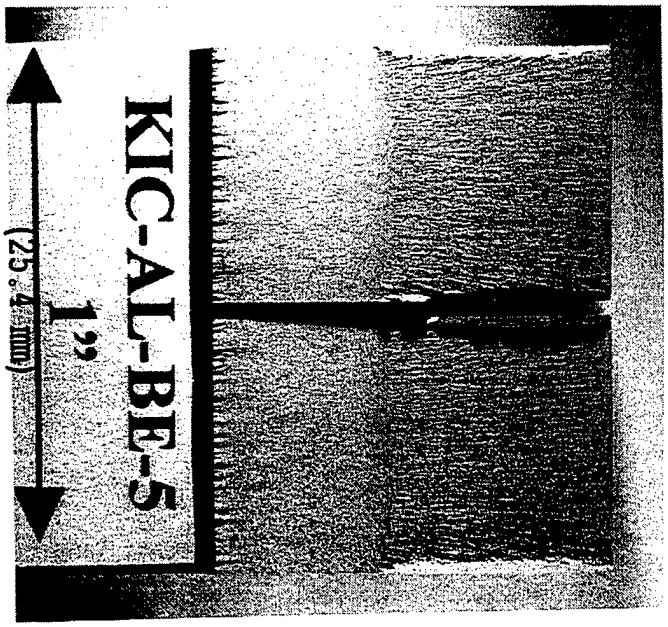

(b) T-L Orientation

Figure A-24: Photographs Depicting the Fracture Surfaces of a Wrought Be-Al Alloy Specimen That Was Fracture-Toughness Tested at Room Temperature

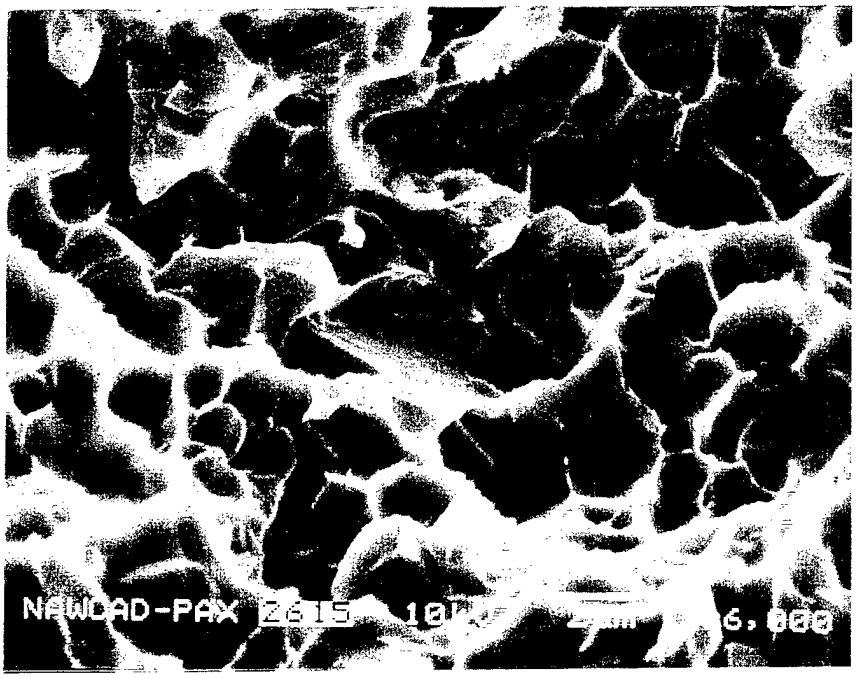

(a) SEM Fractograph

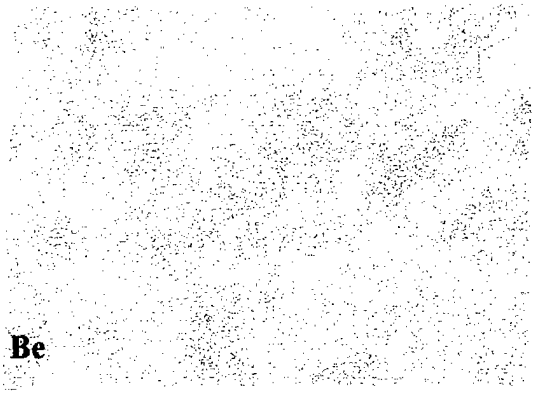

(b) X-ray Dot Mapping of Be

(c) X-ray Dot Mapping of Al

Figure A-25: SEM Micrograph and X-Ray Dot Maps for a Wrought Be-Al Alloy Specimen of L-T Orientation That Had Been Fracture-Toughness Tested at Room Temperature

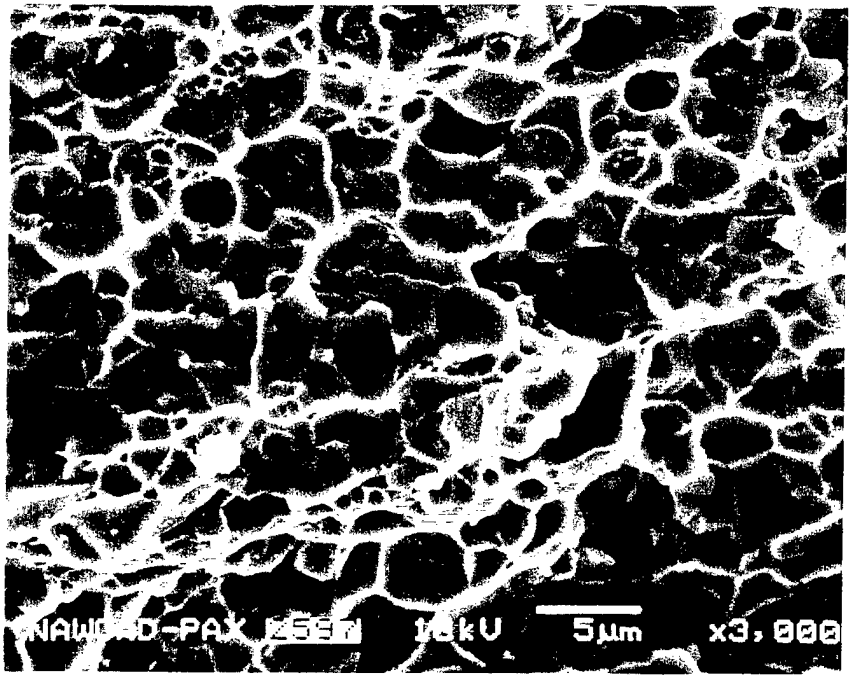

(a) SEM Fractograph

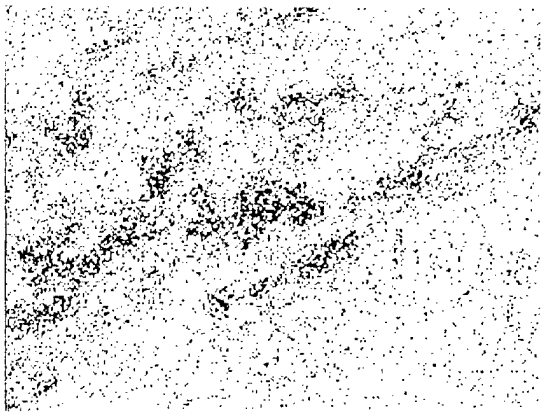

(b) X-ray Dot Mapping of Be

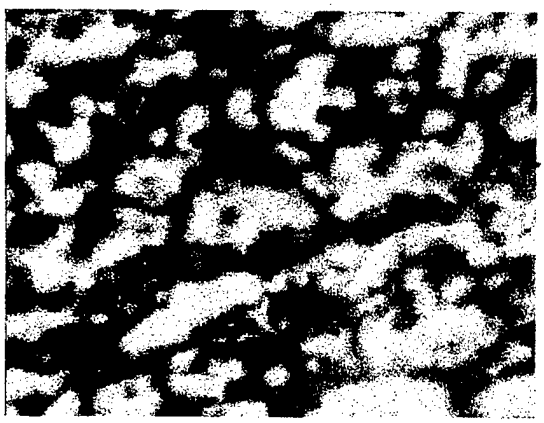

(c) X-ray Dot Mapping of Al

Figure A-26: SEM Micrograph and X-Ray Dot Maps for a Wrought Be-Al Alloy Specimen of T-L Orientation That Had Been Fracture-Toughness Tested at Room Temperature

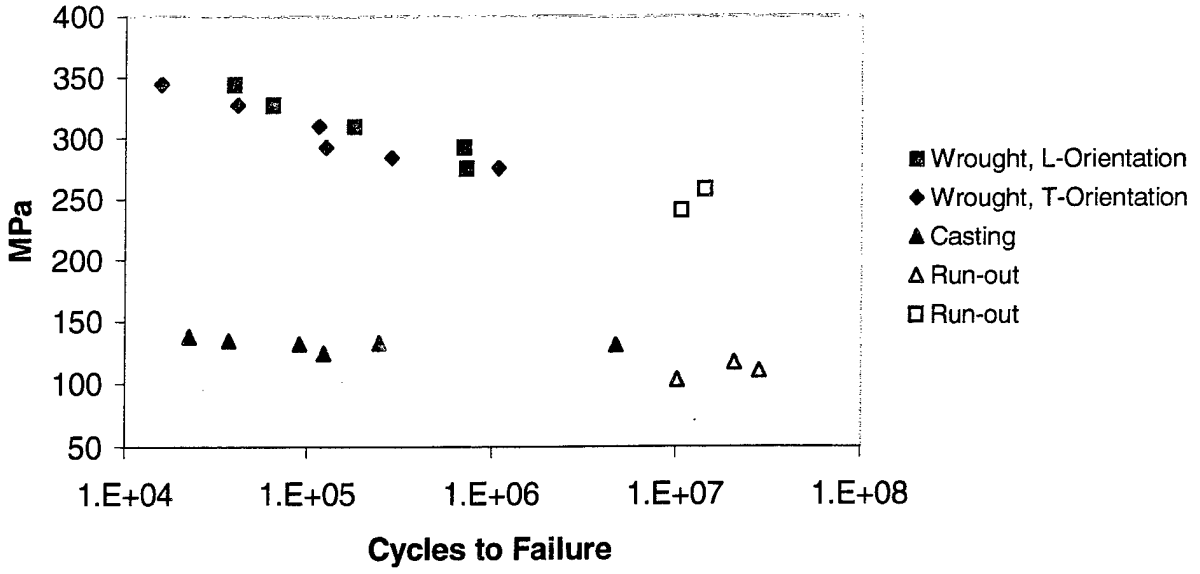

(a) Rectangular Specimen

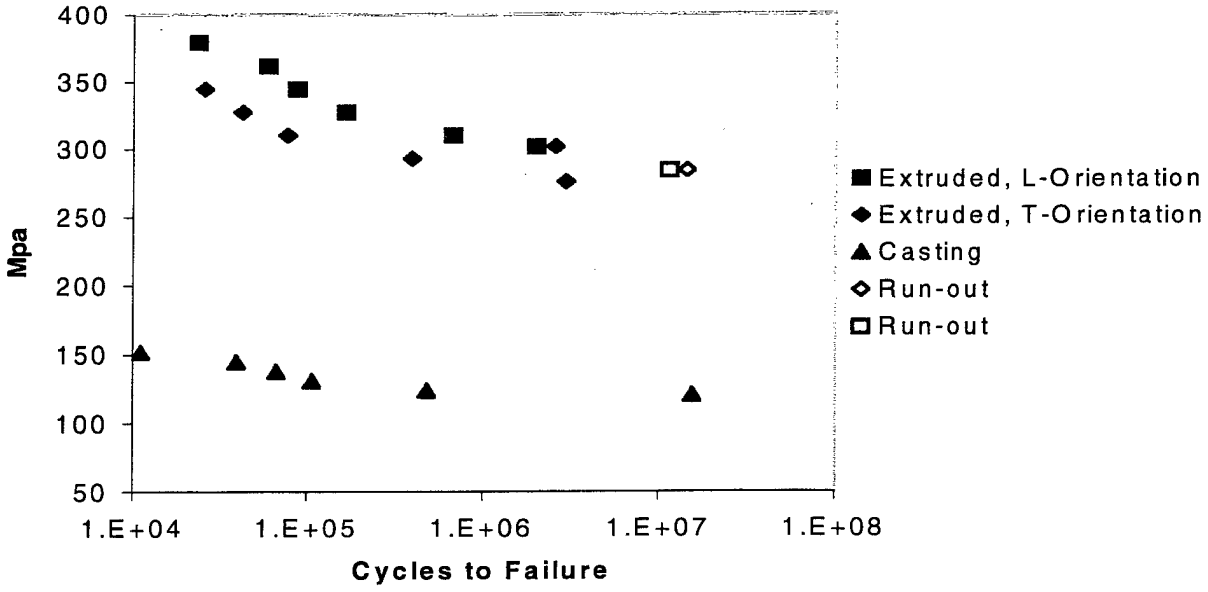

(b) Round Specimen

Figure A-27: Stress-Life (S-N) Curves for Wrought and Cast Be-Al Alloys That Were Fatigue Tested at Room Temperature

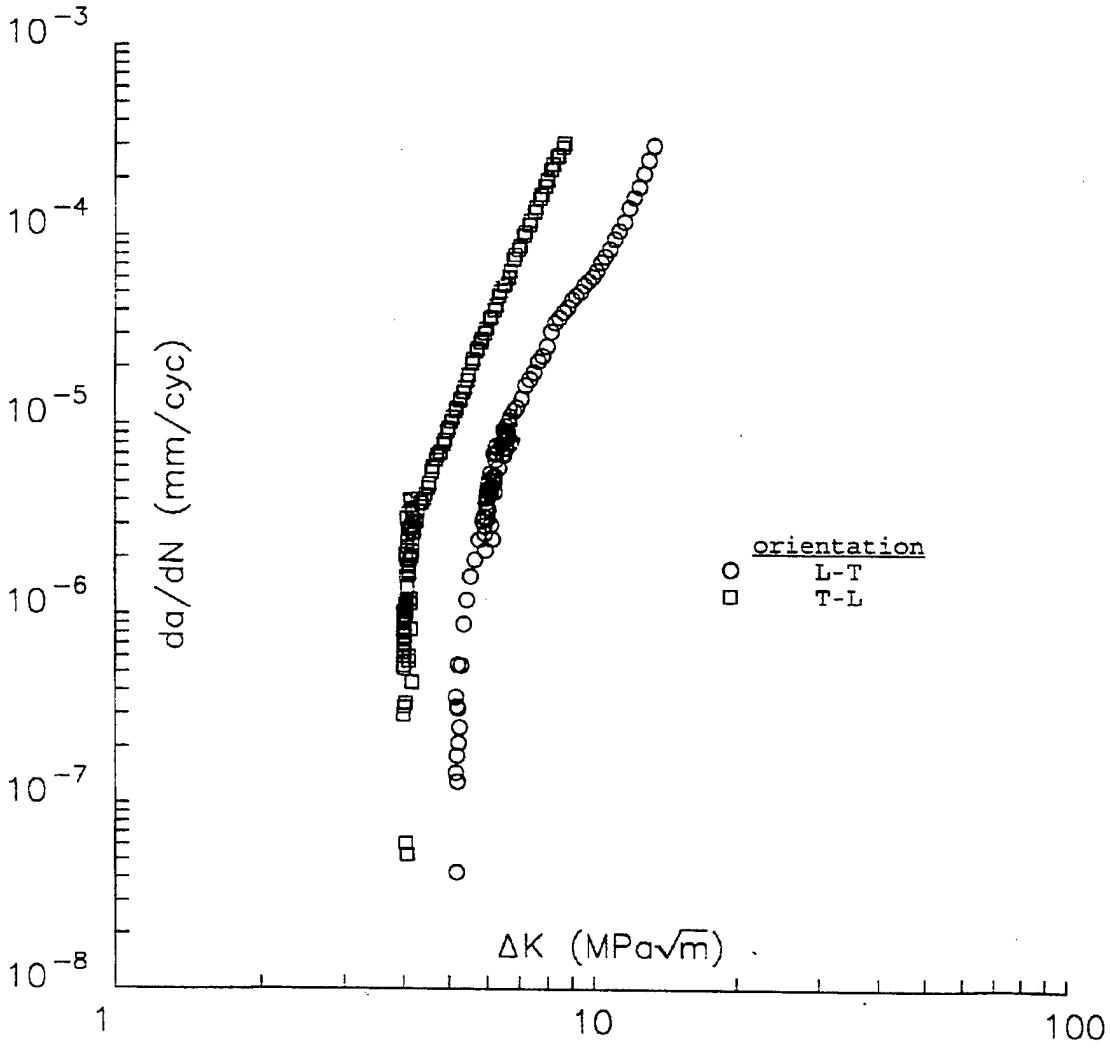

Figure A-28: Variation of Fatigue Crack Growth Rate da/dN With Stress Intensity Range ΔK for Wrought Be-Al Alloy Specimens of L-T and T-L Orientations at a Stress Ratio R = 0.1

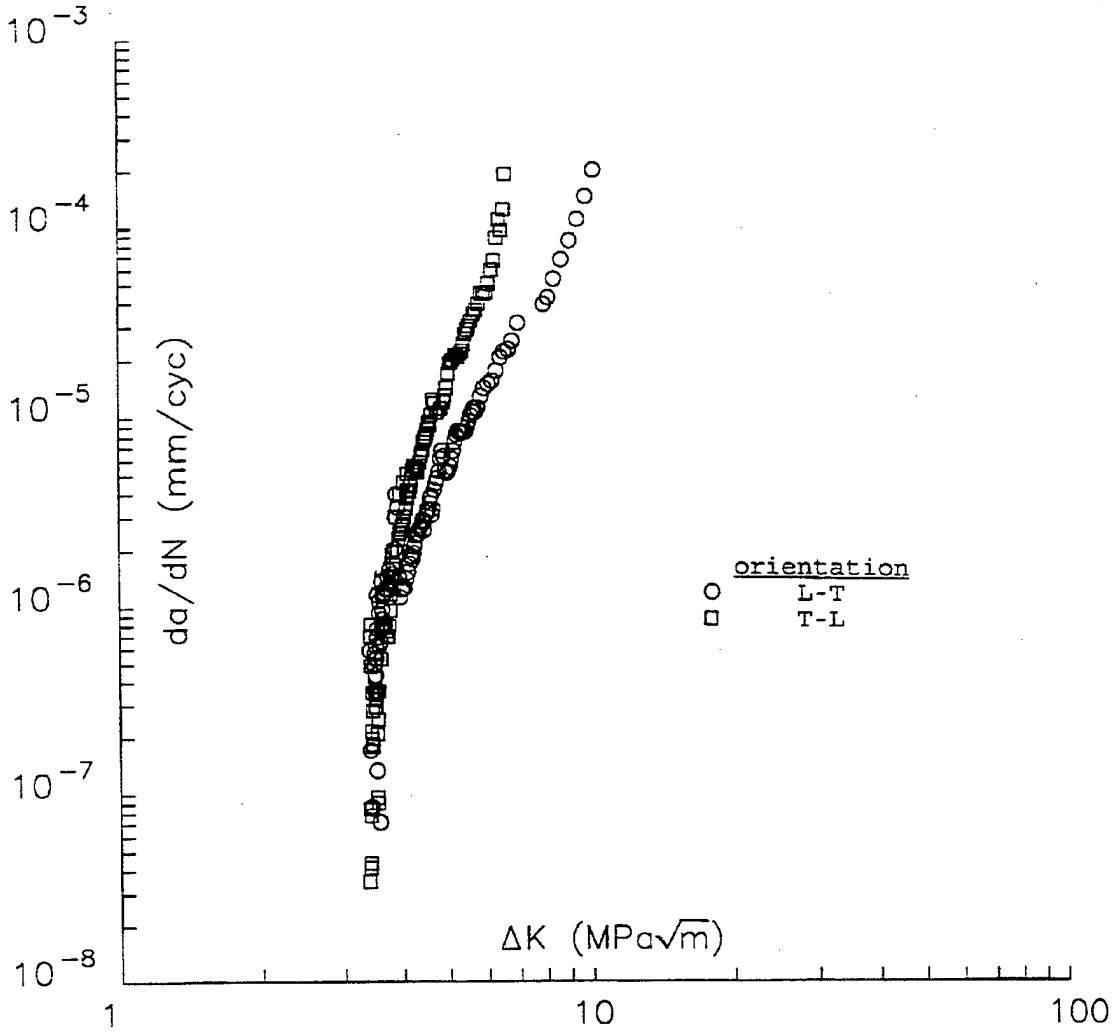

Figure A-29: Variation of Fatigue Crack Growth Rate da/dN With Stress Intensity Range ΔK for Wrought Be-Al Alloy Specimens of L-T and T-L Orientations at a Stress Ratio R = 0.6

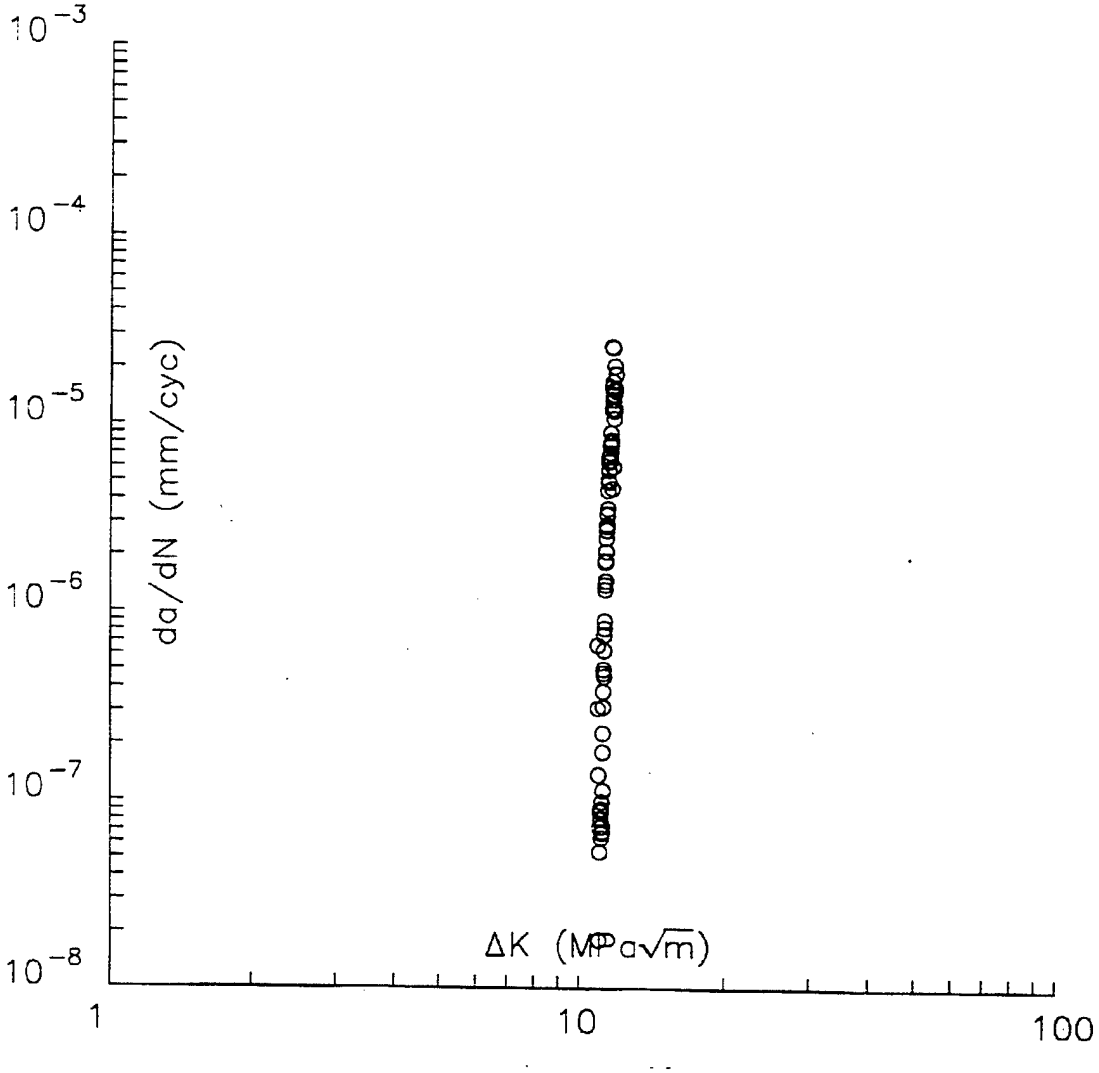

Figure A-30: Variation of Fatigue Crack Growth Rate da/dN With Stress Intensity Range ΔK for a Cast Be-Al Alloy Specimen at a Stress Ratio R = 0.1

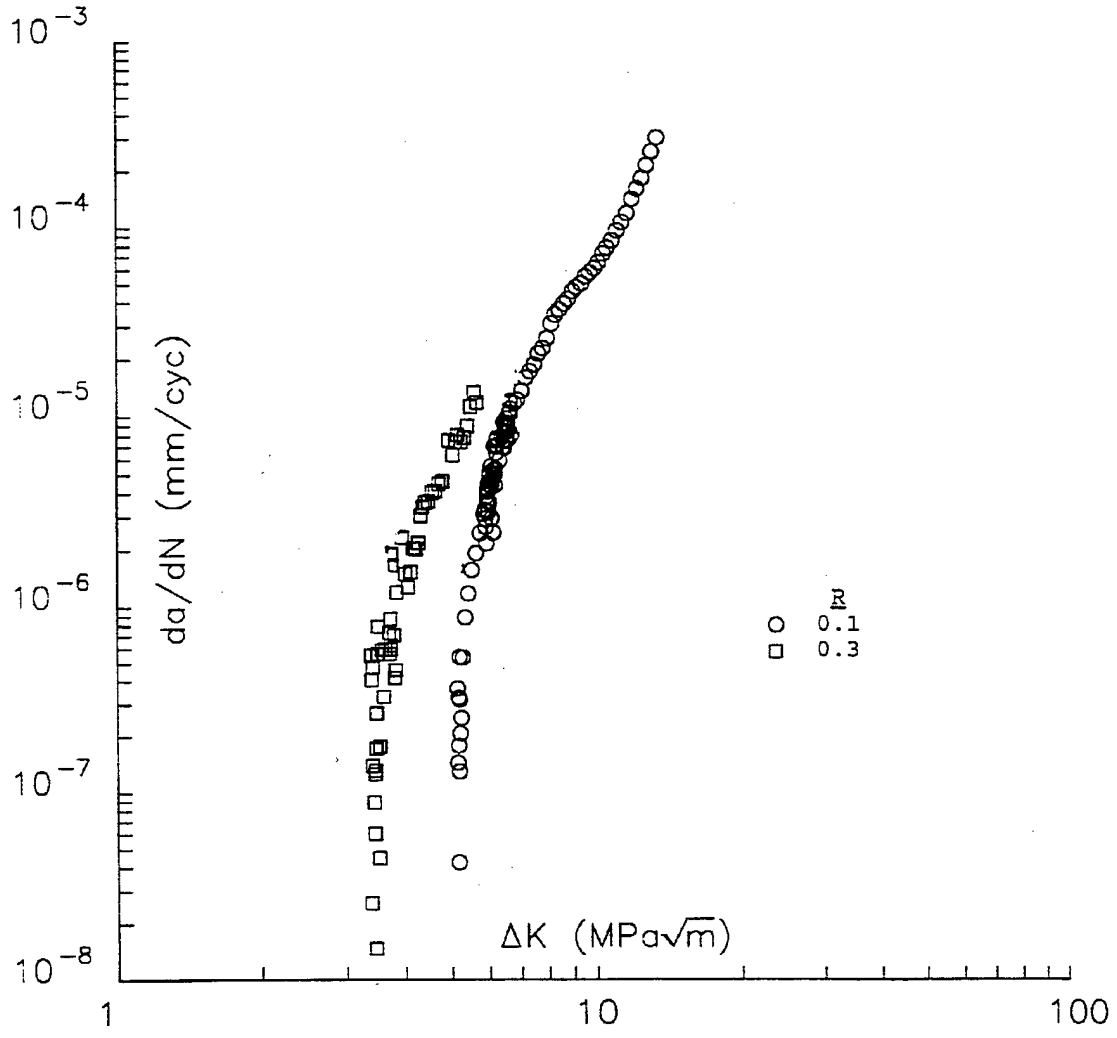

Figure A-31: Variation of Fatigue Crack Growth Rate da/dN With Stress Intensity Range ΔK for Wrought Be-Al Alloy Specimens of L-T Orientation at Stress Ratios R = 0.1 and 0.3

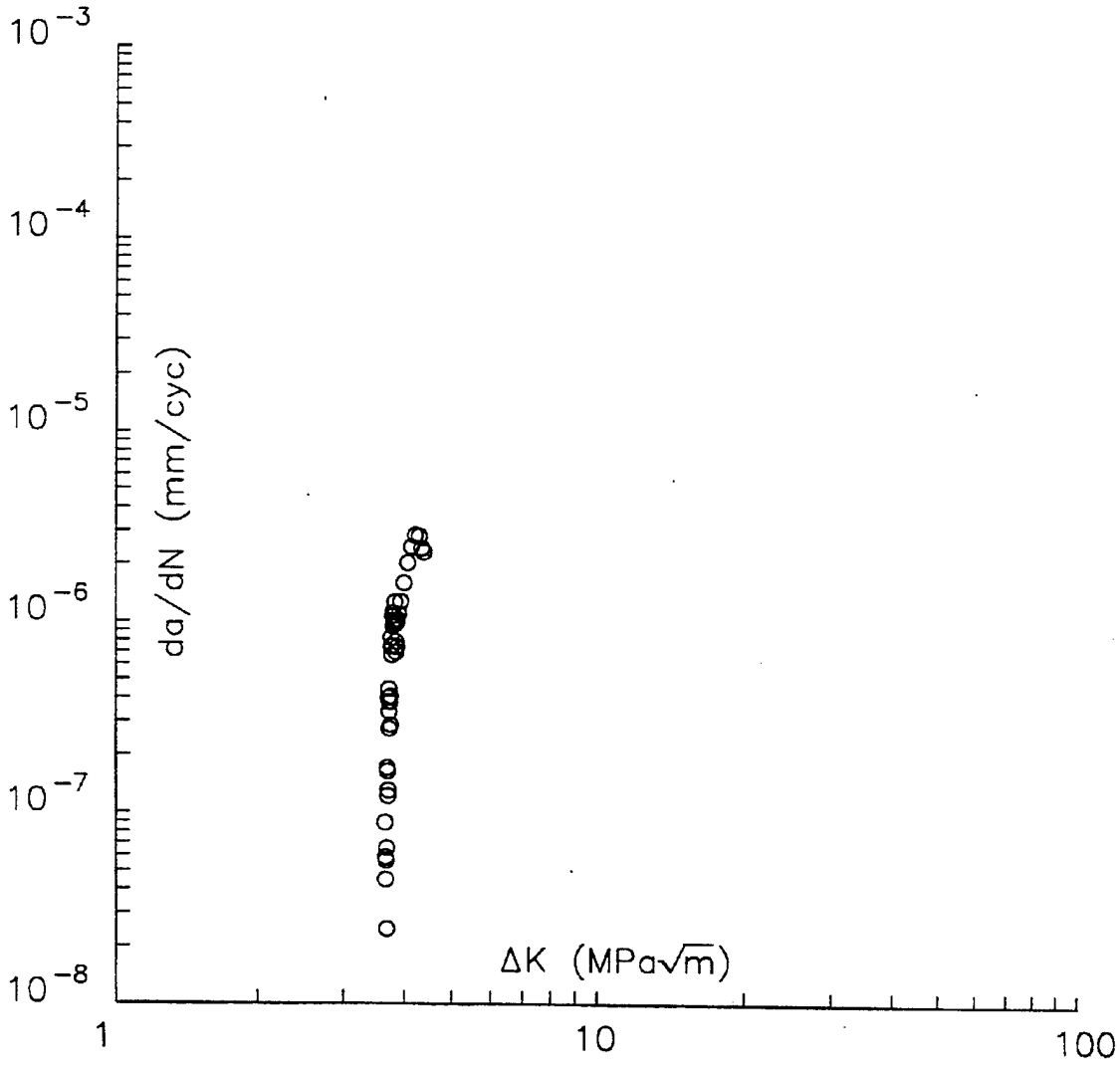

Figure A-32: Variation of Fatigue Crack Growth Rate da/dN With Stress Intensity Range ΔK for a Wrought Be-Al Alloy Specimen of L-T Orientation at a Stress Ratio R = 0.5

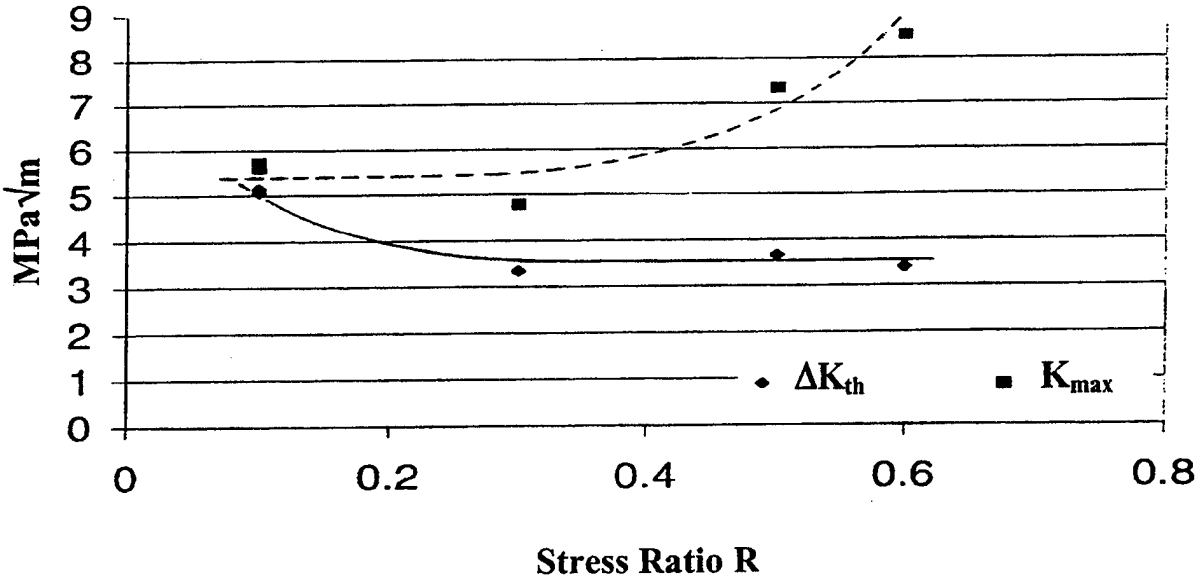

Figure A-33: Variation of Threshold Stress Intensity Range ΔK_{th} and Maximum Stress Intensity K_{max} With Stress Ratio R for Wrought Be-Al Alloy Specimens of L-T Orientation

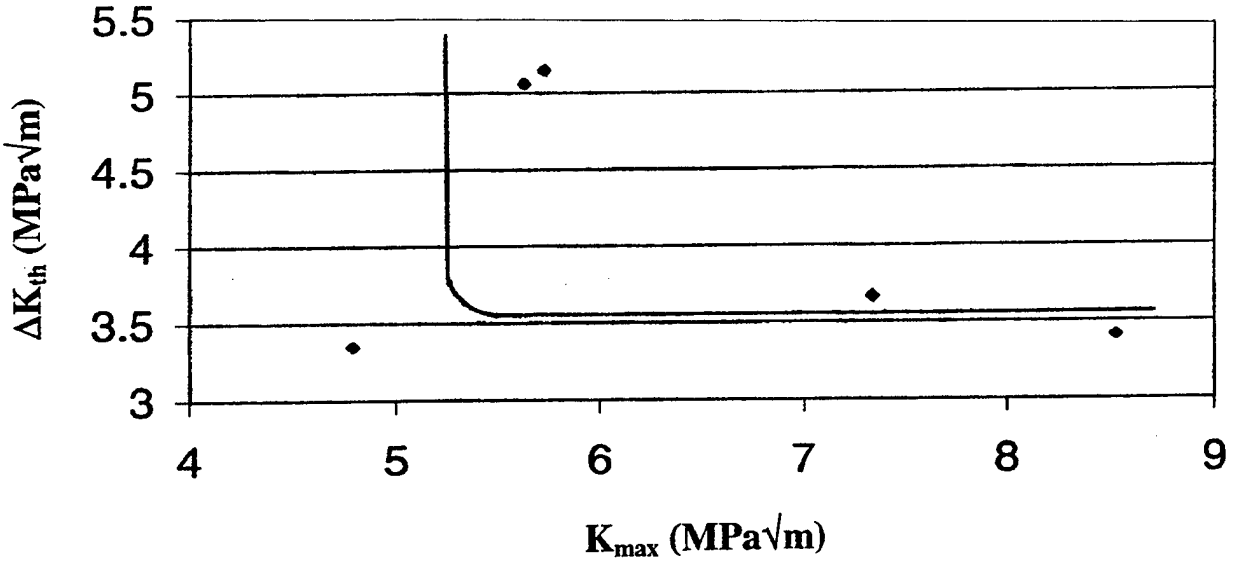

Figure A-34: Fundamental Threshold Curve of Threshold Stress Intensity Range ΔK_{th} Versus Maximum Stress Intensity K_{max} for Wrought Be-Al Alloy Specimens of L-T Orientation

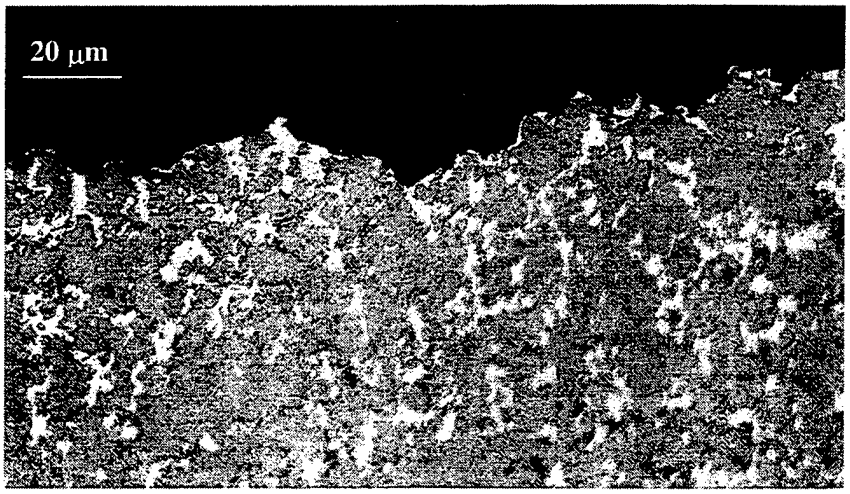

(a) L-orientation

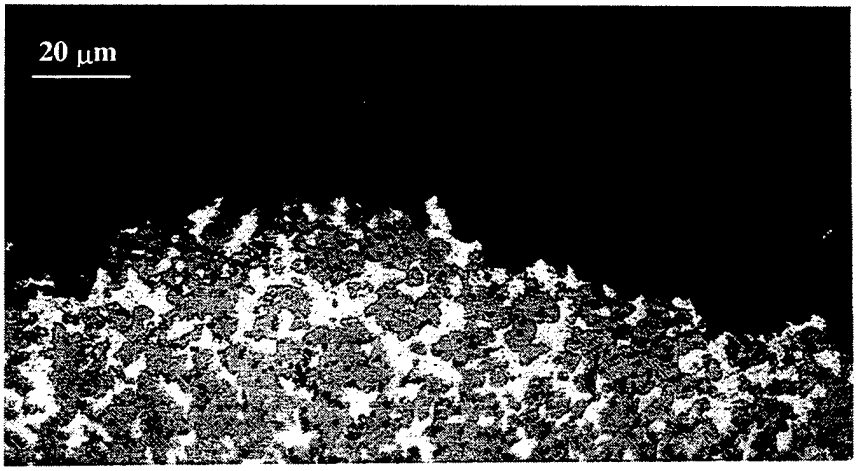

(b) T-orientation

Figure A-35: Optical Micrographs of a Section Through the Fracture Surface Displaying the Fracture Path and Microstructure for Wrought Be-Al Alloy Specimens That Had Undergone Fatigue Testing at Room Temperature

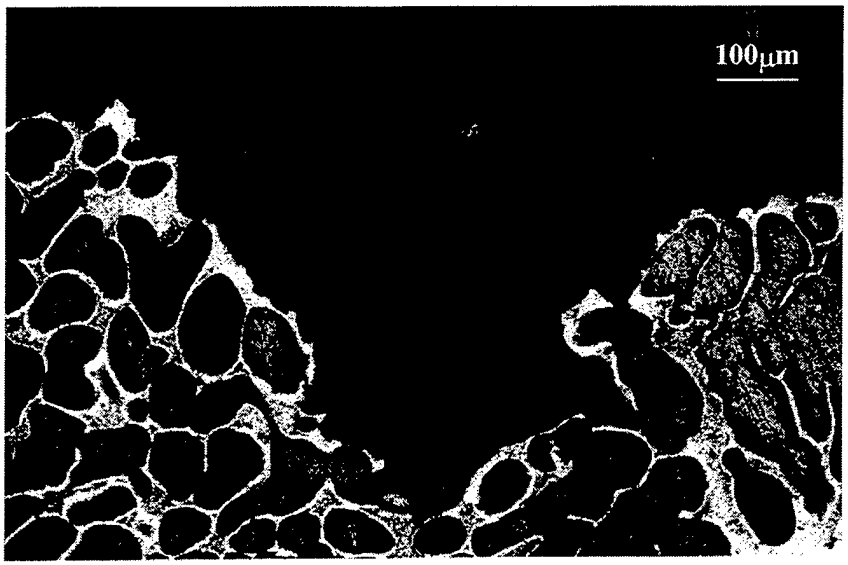

Figure A-36: Optical Micrograph of Section Through the Fracture Surface Depicting the Fracture Path and Microstructure for a Cast Be-Al Alloy Specimen That Had Undergone Fatigue Testing at Room Temperature